



HAL
open science

$^{40}\text{Ar}/^{39}\text{Ar}$ geochronology of crustal deformation

Patrick Monié, Philippe Münch, Gaétan Milesi, Michael Bonno, Arthur Iemmolo

► **To cite this version:**

Patrick Monié, Philippe Münch, Gaétan Milesi, Michael Bonno, Arthur Iemmolo. $^{40}\text{Ar}/^{39}\text{Ar}$ geochronology of crustal deformation. *Comptes Rendus. Géoscience*, 2023, 356 (S2), pp.1 - 29. 10.5802/crgeos.209 . hal-04103276

HAL Id: hal-04103276

<https://hal.science/hal-04103276v1>

Submitted on 23 May 2023

HAL is a multi-disciplinary open access archive for the deposit and dissemination of scientific research documents, whether they are published or not. The documents may come from teaching and research institutions in France or abroad, or from public or private research centers.

L'archive ouverte pluridisciplinaire **HAL**, est destinée au dépôt et à la diffusion de documents scientifiques de niveau recherche, publiés ou non, émanant des établissements d'enseignement et de recherche français ou étrangers, des laboratoires publics ou privés.



INSTITUT DE FRANCE
Académie des sciences

Comptes Rendus

Géoscience

Sciences de la Planète

Patrick Monié, Philippe Münch, Gaétan Milesi, Michael Bonno and Arthur Iemmolo


$^{40}\text{Ar}/^{39}\text{Ar}$ geochronology of crustal deformation

Published online: 15 May 2023

<https://doi.org/10.5802/crgeos.209>

Part of Special Issue: Geodynamics of Continents and Oceans – A tribute to Jean Aubouin

Guest editors: Olivier Fabbri (Université de Franche-Comté, UMR CNRS 6249, Besançon), Michel Faure (Université d'Orléans-BRGM, UMR CNRS 7325, Institut des Sciences de la Terre, Orléans), Laurent Jolivet (Sorbonne Université, IStEP, UMR 7193, Paris) and Sylvie Leroy (Sorbonne Université, CNRS-INSU, IStEP, Paris)

 This article is licensed under the
CREATIVE COMMONS ATTRIBUTION 4.0 INTERNATIONAL LICENSE.
<http://creativecommons.org/licenses/by/4.0/>



*Les Comptes Rendus. Géoscience — Sciences de la Planète sont membres du
Centre Mersenne pour l'édition scientifique ouverte*

www.centre-mersenne.org

e-ISSN : 1778-7025



Geodynamics of Continents and Oceans – A tribute to Jean Aubouin / *Géodynamique des continents et des océans – Hommage à Jean Aubouin*

$^{40}\text{Ar}/^{39}\text{Ar}$ geochronology of crustal deformation

Patrick Monié^{®*, a}, Philippe Münch^{® a}, Gaétan Milesi^{® b}, Michael Bonno^{® a}
and Arthur Iemmolo^{® a}

^a Géosciences Montpellier, Université de Montpellier, CNRS, Université des Antilles,
34095 Montpellier, France

^b GeoRessources, CNRS, Université de Lorraine, Labcom CREGU, 54506
Vandœuvre-lès-Nancy, France

E-mails: patrick.monie@umontpellier.fr (P. Monié), philippe.munch@umontpellier.fr
(P. Münch), gaetan.milesi@univ-lorraine.fr (G. Milesi),
michael.bonno@umontpellier.fr (M. Bonno), arthur.iemolo@umontpellier.fr
(A. Iemmolo)

Abstract. Crustal deformation is characterized by brittle and ductile faults that accommodate at different scales the strain imposed by plate tectonics. The aim of this contribution is to show with the help of different examples how the *in situ* $^{40}\text{Ar}/^{39}\text{Ar}$ dating of synkinematic neocrystallized minerals in ductile shear zones and the step-heating $^{40}\text{Ar}/^{39}\text{Ar}$ dating of synkinematic authigenic clays in fault gouges can bring information on the timing of fault activity. However, due to their complex evolution, interpretation of the argon signature in fault zones requires consideration of several effects among which re- or neocrystallization, inheritance and fluid interaction processes are dominant.

Keywords. Geochronology, Argon, Fault, *In situ* dating, *In vacuo* encapsulation, Clays.

Published online: 15 May 2023

1. Introduction

$^{40}\text{Ar}/^{39}\text{Ar}$ geochronology is one of the most efficient tools for determining the timing of deformation events at different crustal levels, thus it is very useful for constraining the entire development of an orogen from the first stages of its building until its final erosion. Since the first application of this method to terrestrial samples [Fitch et al., 1969], the dating of deformation in crustal rocks has been the focus of many studies, even if until the end of the 80s, few papers report $^{40}\text{Ar}/^{39}\text{Ar}$ ages directly on this topic [e.g. Dallmeyer, 1975, Dallmeyer et al., 1985, Allen and Stubbs, 1982, Monié et al., 1984, Avé Lallemant et al.,

1985, Kligfield et al., 1986, McCaig and Miller, 1986, Keppie and Dallmeyer, 1987, Costa and Maluski, 1988, Hubbard and Harrison, 1989]. However, it is well known that in mountain belts, a large amount of the strain imposed by plate tectonics is accommodated by multiscale deformation zones formed under variable pressure, temperature and fluid regimes. Giving absolute time constraints on deformation is fundamental for determining the propagation of deformation through space and time and unraveling the complex evolution of the different units of an orogen and their juxtaposition [Oriolo et al., 2018]. However, dating of deformation zones remains challenging since most of them record variable P – T strain conditions, resulting in the coexistence of several mineral generations which can be pre-, syn- or postkinematic with respect to the last deformation

* Corresponding author.

[e.g. Lanari *et al.*, 2014]. In addition, the interpretation of $^{40}\text{Ar}/^{39}\text{Ar}$ ages of K-bearing minerals (most often phyllosilicates, more rarely feldspars or amphiboles) is complicated by the fact that deformation introduces microstructural defects in these minerals, favoring their partial or complete fluid-induced recrystallization that have a great effect on the distribution and the retention of argon in their crystalline lattice at the nanometer scale [Naumenko-Dèzes *et al.*, 2021, Villa, 2022]. It should also be stressed that for these deformed rocks the interpretation of the $^{40}\text{Ar}/^{39}\text{Ar}$ data in terms of cooling age or (re)crystallization age remains a subject of debate as well as the mechanisms of age reset during deformation [Villa *et al.*, 2014, Villa, 2016]. Not to mention that there is a wealth of evidence in the literature that the isotopic behaviour of argon is very different for deep/middle crustal and near-surface deformation.

In large and hot orogens, the $^{40}\text{Ar}/^{39}\text{Ar}$ dated minerals of deformed rocks usually reached a state of complete textural, chemical and isotopic equilibrium, and for very slow cooling rate, measured ages record cooling at temperature below the closure temperature of the isotopic systems (in the range 300–550 °C for mica and amphibole), which can occur hundreds of myrs after their crystallization due to slow heat dissipation. In this type of environment with important time-lag between the crystallization of K-bearing minerals and their isotopic closure for argon (e.g. old cratons), the $^{40}\text{Ar}/^{39}\text{Ar}$ method is considered essentially as a method of thermochronology [it dates when a mineral passes through a specific closure temperature, Dodson, 1973, McDougall and Harrison, 1999] that can be combined with other methods (e.g. U–Pb, Sm–Nd, Rb/Sr) to unravel the complex evolution of rocks during their progressive cooling/exhumation. In contrast, for colder (500–300 °C), and/or more localized deformations, the $^{40}\text{Ar}/^{39}\text{Ar}$ age interpretation in deformed zones is not so straightforward, in particular in the case of polydeformed rocks. Different issues have to be considered then: the partial or total resetting of inherited minerals through a combination of (i) thermally activated volume diffusion, deformation and fluid-assisted dissolution–recrystallization processes, (ii) the crystallization, cooling and closure of newly-formed, synkinematic and/or postkinematic minerals and (iii) eventually the presence of excess argon held by fluids. Considering the fulfilled assumptions of

a complete reset of the inherited minerals and the absence of excess argon, $^{40}\text{Ar}/^{39}\text{Ar}$ ages are most often regarded as (re)-crystallization ages and the method is considered as a method of geochronology [it dates mineral (re)crystallization, not cooling; e.g. Mulch and Cosca, 2004, Villa *et al.*, 2014, Di Vincenzo *et al.*, 2016, Villa, 2016, Beaudoin *et al.*, 2020 among many others]. Ideally, the method must be combined with other dating methods, such as the Rb–Sr internal isochron method [e.g. Faure and Mensing, 2004, Rösel and Zack, 2021] or the U–Pb method on monazite or apatite [e.g. Parrish, 1990, Harrison *et al.*, 2002, Chew *et al.*, 2011] which can add additional constraints on the metamorphic and tectonic evolution of rocks deformed at intermediate temperatures. In all these deformed rocks, the $^{40}\text{Ar}/^{39}\text{Ar}$ dating of K-bearing phases is now conducted using mainly lasers with different approaches: step-heating of small mineral populations or single grains, fusion of individual grains, *in situ* ablation within a single grain or at the scale of a small rock section, with a spatial resolution of several tens of microns. As discussed below, this spatial resolution is still insufficient to get a very precise distribution of argon atoms in minerals from sheared zones. However, the combination of these approaches, which has benefited from an improvement in the analytical performance of mass spectrometers over the last ten years, can help to better understand the behavior of argon in deformed rocks and the meaning of $^{40}\text{Ar}/^{39}\text{Ar}$ ages.

For more superficial deformation conditions, many $^{40}\text{Ar}/^{39}\text{Ar}$ studies have successfully focused on fault gouges using authigenic phyllosilicates that form during the activity of these faults in a temperature range corresponding to the muscovite–illite transition (i.e. ductile–brittle transition, ~300 °C) to the illite–smectite transition [~140–90 °C, Freed and Peacor, 1989]. Authigenic phyllosilicates in fault gouges are characterized by their small size (<2 µm), thus corresponding to clay minerals, and usually coexist with inherited K-bearing phases from the host rocks. The dating of these superficial deformations is often rather tricky for several reasons: (1) the size of the neofomed clays requires efficient mineral separation techniques; (2) the proportions of authigenic and inherited phases in the separated grain-size fractions have to be quantified; (3) due to their small size, clay minerals are subject to recoil of ^{39}Ar during irradiation, resulting in an ageing of the samples.

It is shown in the second part of this contribution that these limitations can be overcome and that the situation can sometimes be more complex due to the polyphased activity of faults and various fluid interactions.

Therefore, the present contribution is organized into two main parts addressing specific aspects of $^{40}\text{Ar}/^{39}\text{Ar}$ dating of ductile and brittle deformation in deep and superficial crustal domains through various examples illustrating the complexity of age interpretation in deformed rocks. These examples highlight in particular the benefit of coupling *in situ* laser $^{40}\text{Ar}/^{39}\text{Ar}$ analyses with detailed microstructural and petrological observations for the study of ductile deformations and the reconstruction of P - T - d - t (pressure-temperature-deformation-time) paths. The second section is focused on brittle deformation and fault gouges and shows the advantages of coupling geochronology and thermochronology in orogenic belts.

2. $^{40}\text{Ar}/^{39}\text{Ar}$ geochronology of ductile deformation

2.1. Some methodological aspects

It is beyond the scope of this contribution to present the technical details of the $^{40}\text{Ar}/^{39}\text{Ar}$ method that can be found in the reference book of McDougall and Harrison [1999] and more recently in Jourdan *et al.* [2014] or Schaen *et al.* [2021]. In a simplified way, the method is derived from the ^{40}K - ^{40}Ar method, ^{39}Ar being a proxy of the quantity of ^{40}K after fast neutron irradiation in a nuclear reactor and the age directly dependent on the ratio between the two argon isotopes and the fluence of neutrons calculated from argon isotopes released by co-irradiated flux monitors. Technical aspects of the $^{40}\text{Ar}/^{39}\text{Ar}$ method, which concern the age of the monitors, decay constants, argon recoil effects, or the current $^{40}\text{Ar}/^{36}\text{Ar}$ atmospheric ratio, are still under debate but will not be addressed here [Schaen *et al.*, 2021]. Soon after the inception of the $^{40}\text{Ar}/^{39}\text{Ar}$ method [Merrihue and Turner, 1966], laser microprobe $^{40}\text{Ar}/^{39}\text{Ar}$ analyses were first performed on lunar breccias [Megrue, 1973] and some years later on terrestrial samples [York *et al.*, 1981, Maluski and Schaeffer, 1981] using continuous or pulsed lasers for a sampling of small material amount (<milligram). From there on, many

laboratories worldwide developed this technique using different lasers that can be coupled now with very sensitive mass spectrometers to produce very precise and reproducible $^{40}\text{Ar}/^{39}\text{Ar}$ ages (from 3.5 Ga to some ka) on K-bearing terrestrial samples. The method is under constant improvement and addresses a wide range of geological processes such as metamorphism, magmatism, hydrothermalism, diagenesis, weathering, deformation . . . Its range of applications is then very large from geodynamics, paleomagnetism, mineral and geothermal resources, seismic risk but also paleontological or climate evolution.

As indicated in the introduction and schematized on Figure 1, different methods of argon extraction can be achieved with the different types of laser. This includes first the step-heating degassing of single grains or micro-populations of K-bearing samples by increasing progressively the power of a continuous infrared CO_2 laser beam applied to the grains. An age is calculated at each argon release increment and the whole step data is portrayed in an age spectrum and inverse isochron plot. In some instances, Ca/K and Cl/K vs. age correlation plots can help to better differentiate the various argon reservoirs that can coexist in samples with a complex history of metamorphic-deformation processes and fluid interactions [e.g. Mulch *et al.*, 2005, Simon-Labric *et al.*, 2009, Allaz *et al.*, 2011].

However, it is well-known that hydrous phases such as micas and amphiboles do not release argon by volume diffusion when heated under vacuum because of their metastability and that age spectra do not reflect the true argon distribution in the dated minerals [e.g. Sletten and Onstott, 1998, Lo *et al.*, 2000, Villa, 2021]. This is well supported by the different studies comparing step-heating and *in situ* laser probe experiments, for instance in the case of slow cooling terranes, excess argon contamination, thermal or tectonic overprint [e.g. Phillips, 1991, Hodges *et al.*, 1994, Monié *et al.*, 1994, Kellet *et al.*, 2016]. Caution should therefore be exercised when interpreting step heating results and, in case of doubt, a comparison with other modes of argon extraction or other isotope chronometers may be useful.

Continuous laser beams can also be used for the total fusion of individual grains [e.g. Uunk *et al.*, 2018, Gemignani *et al.*, 2018, Porkoláb *et al.*, 2022]. Ages are usually reported in probability or Kernel density plots [Ludwig, 2012, Vermeesch, 2018,

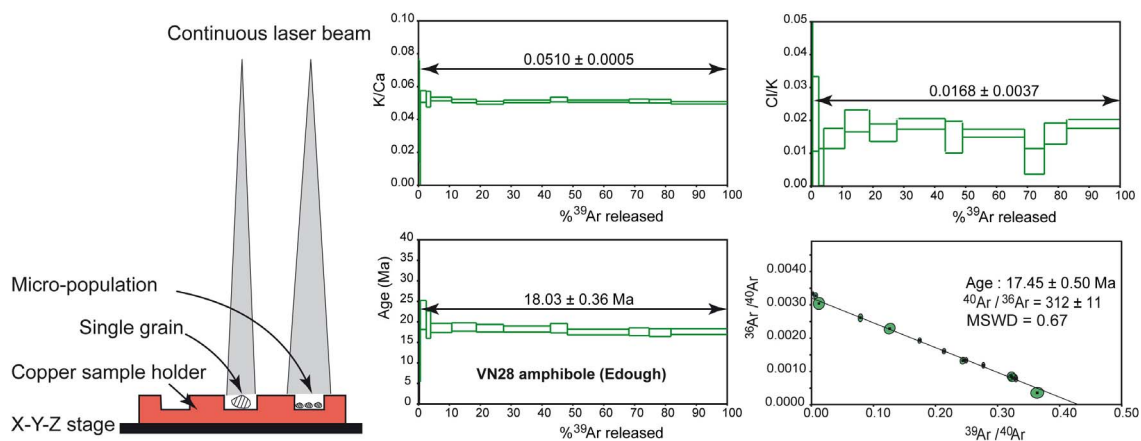


Figure 1. From left to right, (1) different modes of laser microprobe step-heating of a single grain or micro-population, (2) age and K/Ca spectra and (3) Cl/K spectrum and inverse isochron plot for a homogeneous amphibole micro-population [Fernandez *et al.*, 2020].

Schaen *et al.*, 2021] in order to identify the different age populations in a rock sample (Figure 2), a method that requires a large number of analyses to get statistically meaningful peak ages. This approach, for which the main criterion of grain selection is their large size, can be used to better interpret discordant age spectra from complex polymetamorphic tectonites.

However, in deformation zones where phyllosilicates are the main target of $^{40}\text{Ar}/^{39}\text{Ar}$ analyses, micas of different origin, size and chemistry can occupy different microstructures and the distinction between not reset, partially reset, totally reset and newly crystallized populations is not always straightforward, without discarding the problem of excess argon contamination. The $^{40}\text{Ar}/^{39}\text{Ar}$ laser fusion dating of single grains does not always resolve these complex isotopic situations since, in general, few attention is paid to the grain-size effect on the age distribution or to the chemical heterogeneities within and between micas. By contrast, the *in situ* $^{40}\text{Ar}/^{39}\text{Ar}$ method has the advantage to preserve the textural and chemical relationships between the different mineral generations in polydeformed rocks and to establish correlations between ages, mineral fabrics and petrology at the scale of several tens of microns, corresponding to a volume large enough to measure accurately the different argon isotopes on the mass spectrometer (typically a square of $150 \times 150 \mu\text{m}$ and 20 to $50 \mu\text{m}$ deep). Different pulsed lasers have been used since the first

dating of terrestrial samples 40 years ago, including infrared ruby lasers, argon-ion visible lasers, ultraviolet Nd-YAG lasers and more recently UV excimer lasers that provide the best spatial resolution for *in situ* analyses. These analyses that can be realized at the scale of a single grain if it is large enough to perform several ablations inside (Figure 3), have the potential to resolve core to rim zonation or other kinds of age distribution due to slow cooling or partial resetting by thermally activated diffusion or chemical exchanges and recrystallization [e.g. Phillips and Onstott, 1988, Scaillet *et al.*, 1990, Hames and Hodges, 1993, Hames and Bowring, 1994, Monié *et al.*, 1994, for some of the oldest references].

However, for most *in situ* studies of deformed rocks, dating experiments are not realized at the scale of a single mineral, but at the scale of a portion of thin section (Figure 4) in order to deconvolute the complete history of deformation and metamorphism.

In an orogen, ductile shear zones concentrate a large part of deformation and, because of their efficient reactivity, phyllosilicates are ideal candidates for recording the short- and long-term evolution of faults through their chemistry (major elements, trace elements and fluid composition), grain size and isotopic ages. Thus, microscope observation of thin sections usually is a first step to identify the different generations of pre-, syn- and postkinematic minerals suitable for dating (Figure 5).

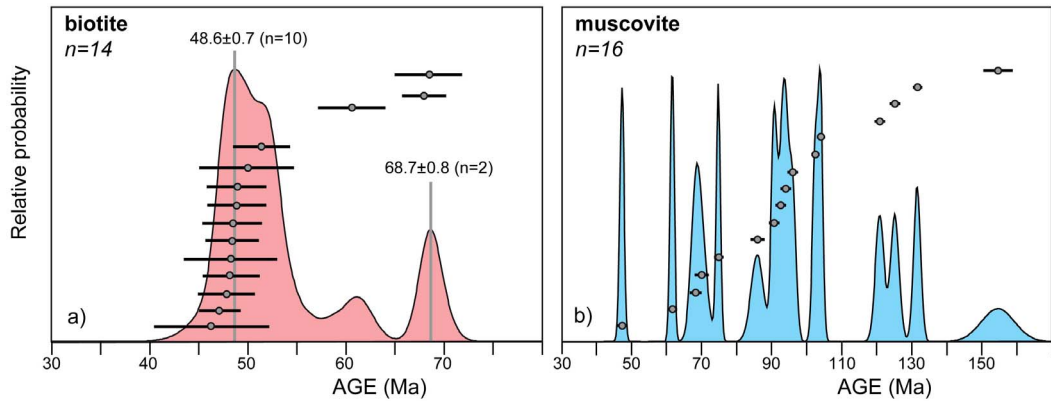


Figure 2. Distribution of total fusion ages for (a) a homogeneous population of biotite with few grains showing inherited or excess argon and (b) a strongly heterogeneous population of muscovite showing decreasing amount of argon resetting from left to right [Cap de Creus samples, Monié *et al.*, 2018].

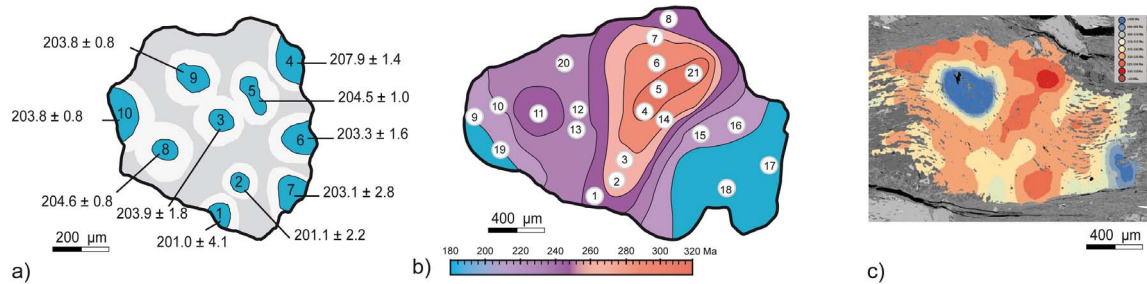


Figure 3. *In situ* ages obtained inside single mica grains using an argon-ion visible laser (a,b) and a quintupled UV laser (c). (a) Homogeneous Triassic ages inside a high-pressure phengite from Turkey [Okay and Monié, 1997]; (b) core-rim age zonation in a thermally overprinted Variscan magmatic biotite from the Eastern Pyrénées [Monié *et al.*, 1994]; (c) irregular age zonation in a partially chloritized Variscan biotite from the Cévennes schists [Montmartin, 2021].

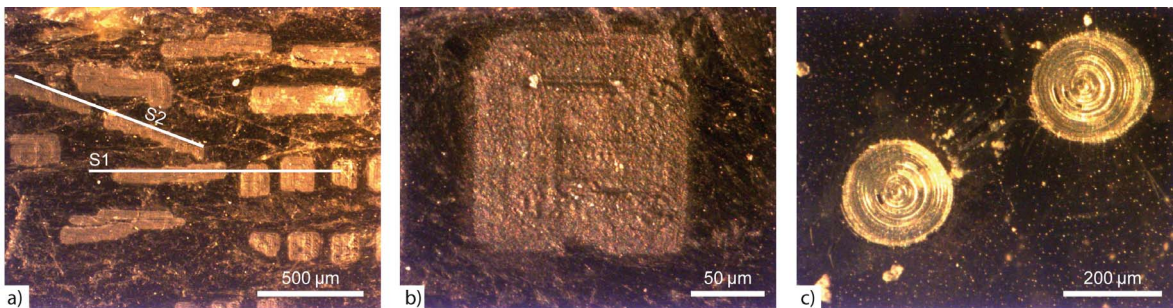


Figure 4. Different modes of *in situ* argon extraction with a quadrupled UV laser. (a) Typical surface of gneiss thick section after lasing. The micas aligned along the two schistosity S1 and S2 have been dated. (b) Detailed view of the surface of a mica after a fast laser rastering. The depth of the pits is less than 10 μm . (c) Laser drilling on a muscovite to a depth of about 50–70 μm . Note the white ejecta around the craters.

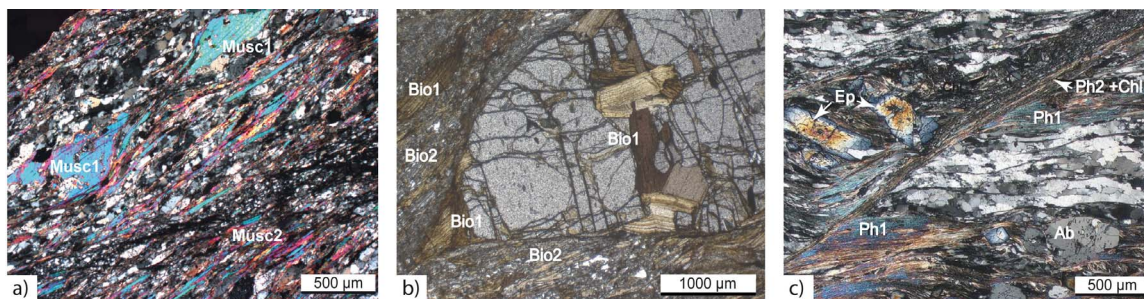


Figure 5. Examples of textural relationships in metamorphic tectonites, from left to right, (a) micaschist with prekinematic large muscovite (Musc1) in a fine-grained matrix of quartz–feldspar–muscovite (Musc2) [Cap de Creus massif, Monié *et al.*, 2018]; (b) partially reworked garnet–sillimanite–quartz–biotite (Bio1) gneiss in a matrix of quartz and fine-grained biotite (Bio2). Note the different habits of prekinematic biotite as clasts in the new foliation, in a garnet pressure-shadow and in a crack inside garnet [Agly massif, Aumar *et al.*, 2022]; (c) albite–quartz–epidote–phengite (Ph1) micaschist crosscut by a chlorite–phengite (Ph2) shear band [Andros island, Huet *et al.*, 2015].

The examples of Figure 5 illustrate the importance of identifying the different textural habits of the minerals that can be dated by *in situ* $^{40}\text{Ar}/^{39}\text{Ar}$ laser analyses. Two samples from Cap de Creus and Agly massifs (Figure 5a,b) highlight the evolution of grain size in tectonites, with prekinematic micas being usually larger than synkinematic matrix micas. In most tectonites, the fine-grained matrix consists of two mica types: a first type resulting from a strong mechanical reduction in size of part of the inherited micas (comminution), and a second type that is newly formed by a fluid-enhanced dissolution–precipitation mechanism. Therefore, the matrix micas can only give homogeneous ages if those of the first type have undergone a complete isotopic resetting of their K–Ar chronometer during comminution, which is closely dependent on the crustal deformation conditions (temperature, pressure, duration, fluid behaviour, open/closed system behaviour of the host rock...). For the third sample from Andros island (Figure 5c), a first generation of synkinematic phengite Ph1 is aligned along the main foliation while synkinematic phengite Ph2 is also present in association with chlorite along a late shear band. However, it is likely that together with the neocrystallization of phengite Ph2, some early phengite Ph1 was caught by the shear band. Therefore, *in situ* $^{40}\text{Ar}/^{39}\text{Ar}$ mica dating in this kind of microstructure can constrain the last deformation age only if micas inherited from the main foliation have been fully

reopened (or recrystallized) along the shear band, which is also dependent on the deformation conditions. Insofar as the ages of the different generations of synkinematic micas can be interpreted as reflecting crystallization ages (see below), they can provide an indication of how long a shear zone remains active [e.g. Schneider *et al.*, 2012].

After this first step and before dating, it is fundamental to consolidate the microstructural observations by a petrological study of the mineral assemblages to constrain the P – T conditions of the different deformation episodes. Detailed EPMA analyses coupled with SEM imaging or EDS mapping are the main tools used to decipher the chemical composition of datable minerals, and to reveal at the scale of a thin section inter- and intra-grain variations related to more or less complex P – T – D paths recorded by the tectonites during the orogenic cycle. Figure 6 shows some examples of chemical data that can be served as a guide to perform texturally and chemically-controlled *in situ* $^{40}\text{Ar}/^{39}\text{Ar}$ analyses in deformed crustal rocks.

Therefore, before *in situ* $^{40}\text{Ar}/^{39}\text{Ar}$ dating, a detailed petro-structural study of the samples that are the most representative of the study area is highly recommended and depending on the goals pursued, the study should focus on texturally and chemically homogeneous samples dominated by a single K-bearing mineral population (early or late) or on more complex samples that record several phases of

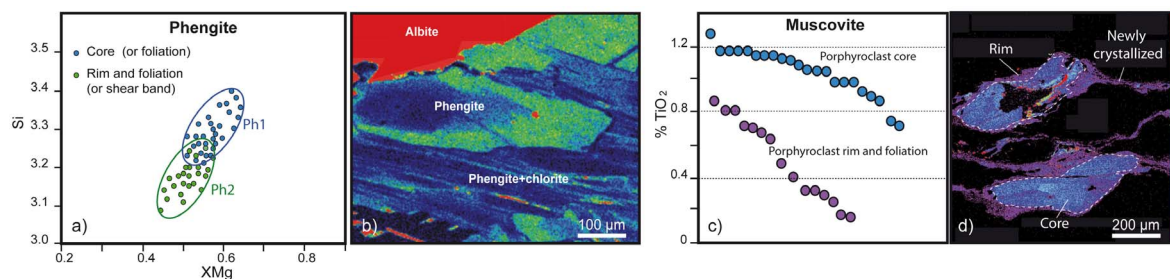


Figure 6. Examples of mica chemical variations that can be observed in metamorphic rocks: (a) EPMA analyses of phengites in a retrogressed high-pressure (HP) micaschist from Iran with two populations that can correspond to the situation in Figure 6b [core-rim zoning, Rossetti *et al.*, 2017] or that in Figure 5c (HP foliation crosscut by lower pressure shear band); (b) SEM imaging of a zoned phengite with a celadonite-rich core and a poorer rim; (c) EPMA analyses of TiO_2 content of muscovite in an orthogneiss from the South Armorican Massif. Note the high Ti content in the mica core compared to the rim and to the newly crystallized muscovite along the foliation; (d) X-ray mapping of Ti content in muscovites from Figure 6c [Turrillot *et al.*, 2011].

deformation–(re)crystallization (Figure 6). As shown on Figure 4, the *in situ* $^{40}\text{Ar}/^{39}\text{Ar}$ method has the ability to provide ages with a spatial resolution of about $100\text{--}150\ \mu\text{m}^2$ that is enough to get first-order data on the homogeneity or heterogeneity of dates at the scale of a thick section. It is likely that this spatial resolution will be improved in the future with the advent of increasingly sensitive mass spectrometers. However, many studies have shown that reliable textural–chemical–age relationships can be already established with current $^{40}\text{Ar}/^{39}\text{Ar}$ spatial resolution [e.g. Maluski and Monié, 1988, Kramar *et al.*, 2001, Agard *et al.*, 2002, Mulch and Cosca, 2004, Mulch *et al.*, 2002, Augier *et al.*, 2005, Mulch *et al.*, 2005, Di Vincenzo *et al.*, 2007, Schneider *et al.*, 2012, Angiboust *et al.*, 2015, Bellanger *et al.*, 2015, Di Vincenzo *et al.*, 2016, Kellet *et al.*, 2016, Scharf *et al.*, 2016, Berger *et al.*, 2017, Laurent *et al.*, 2017, Angiboust *et al.*, 2018, Tan *et al.*, 2019, Beaudoin *et al.*, 2020, Ghignone *et al.*, 2021, Di Vincenzo *et al.*, 2022].

2.2. Age interpretation

From the earliest applications of the method to the dating of magmatic and metamorphic rocks, a notion of isotopic system closure temperature emerged and was formulated by Dodson [1973] on the basis of volume diffusion laws. During cooling, a K-bearing mineral will start to accumulate radiogenic argon at a certain temperature T_1 and will become a closed

system at lower temperature T_2 , the temperature interval $T_1\text{--}T_2$ defining what is called the partial retention zone. The closure temperature T_c of this mineral lies within this partial retention zone whose range is dependent on the cooling rate. For fast cooling rates (e.g. volcanic rocks), T_1 , T_2 and T_c are very close and the $^{40}\text{Ar}/^{39}\text{Ar}$ ages can be interpreted to date crystallization. This is the case of the sanidine standards from volcanic rocks used to monitor the fast neutron flux during sample irradiation whose $^{40}\text{Ar}/^{39}\text{Ar}$ ages agree with U–Pb zircon ages [e.g. Fleck *et al.*, 2019]. It is also common to observe this concordance of U–Pb and $^{40}\text{Ar}/^{39}\text{Ar}$ ages for granites emplaced in the upper crust, with micas revealing no core to rim age zonation due to fast cooling [e.g. Brichau *et al.*, 2007]. Note that in deformed rocks from the mid-upper crust, synkinematic minerals formed at temperatures close to $500\text{--}550\ ^\circ\text{C}$ can also provide similar monazite U–Pb and $^{40}\text{Ar}/^{39}\text{Ar}$ mica ages interpreted as crystallization ages [e.g. Aumar *et al.*, 2022]. For very slow cooling low- to mid-crustal deformed rocks (e.g. large Proterozoic cratons), the partial retention zone is usually very large and the time elapsed between the crystallization of K-bearing minerals and their complete closure for argon diffusion can reach several hundred million years. This results in core to rim age zonations reflecting a progressive closure of the K–Ar chronometer [e.g. Hodges *et al.*, 1994, for muscovite] that can be modeled using thermal volume diffusion laws [e.g. Warren *et al.*, 2012, Skipton

et al., 2018]. Indeed, by contrast with the fast cooling setting, the core to rim age range represents a segment on the cooling path which length is dependent on grain size, cooling rate and residence time of the crustal rocks at given temperature and pressure, diffusion parameters of the mineral species under consideration and the open behavior of the host rock. Available K–Ar systems permit to cover a continuous range of closure temperatures from about 550 °C (amphibole) to 150 °C (K-feldspar) that have been determined empirically, theoretically and experimentally. To reconstruct the T – t cooling trajectory above and below this temperature range, complementary geochronological and thermochronological studies using U–Pb, Sm–Nd, Rb–Sr, fission tracks and U–Th–Sm/He methods are required. Therefore, in very slowly cooled high-temperature rocks with a single episode of deformation at peak temperature, the ages provided by the $^{40}\text{Ar}/^{39}\text{Ar}$ method can only be considered as minimum estimates of the deformation age. When different deformation episodes occur during cooling, thermo-barometric analysis of synkinematic mineral assemblages allows in principle to assign the different deformation stages along the P – T path. If these deformations occur at temperatures close to the isotopic closure temperatures of argon chronometers, *in situ* $^{40}\text{Ar}/^{39}\text{Ar}$ dating of the synkinematic K-bearing minerals can constrain the timing and duration of tectonic events and the rate of deformation propagation or localization, provided that the dated minerals do not contain inherited or excess argon which can be resolved by *in situ* intra- and inter-grain analyses. However, at present, large uncertainties remain on the closure temperature of the mineral species used for $^{40}\text{Ar}/^{39}\text{Ar}$ dating, due to the lack of precision of the experimentally determined diffusion parameters, the validity of diffusion experiments themselves as well as the influence of the multiple parameters that can affect argon retentivity in the minerals during cooling (chemical composition, pressure, lithology, open/closed behavior of host rock, fluid composition and behaviour...). This is true in particular for the white mica group for which a large range of closure temperature is suggested by different studies, from 350 to 550 °C or more [e.g. Hames and Bowring, 1994, Harrison et al., 2009, Nteme et al., 2022], a range which remains an area for future exploration. As a consequence, the reconstruction of P – T – D – t

path in polydeformed high-temperature rocks using $^{40}\text{Ar}/^{39}\text{Ar}$ data can suffer from this indetermination of the retention properties of the dated minerals and for this purpose the use of multiple geochronometers is highly recommended. It is important also to mention that the mechanisms involved during the closure of an isotopic system may be different from those leading to its resetting. In particular, various $^{40}\text{Ar}/^{39}\text{Ar}$ laser probe studies of polydeformed high-temperature rocks showed that a mineral can survive temperatures well in excess of its closure temperature without loss of radiogenic argon [e.g. Kelley et al., 1997, Di Vincenzo et al., 2001, Maurel et al., 2003, Schneider et al., 2008]. This is interpreted to reflect a closed system behaviour of the host rock with no or limited fluid-rock interaction due to intrinsic rock properties (mineralogy, porosity, deformation, interstitial fluid amount) and conditions of overprinting (temperature, pressure, duration, fluid behavior). This is to say that in a polyphased context, the interpretation of ages strictly in terms of crossing a given temperature barrier in one direction or the other can be debated without a proper understanding of the variable parameters that control the closure and opening of the chronometers being used. This is a highlight made several years ago by Chopin and Maluski [1980] in their studies of some high-pressure rocks of the Western Alps and subsequently validated by many geochronological works [see Agard et al., 2002, Ghignone et al., 2021 for *in situ* $^{40}\text{Ar}/^{39}\text{Ar}$ studies in the same area, or McDonald et al., 2016 for the HP gneisses of Norway].

For deformations that occur at lower temperature, from 500 °C to the ductile–brittle transition at 300 °C, it is frequent that different generations of K-bearing minerals (re-)crystallized along the P – T – D – t path which renders the interpretation of $^{40}\text{Ar}/^{39}\text{Ar}$ ages somewhat difficult due to the interaction of several effects of grain deformation during shearing, chemical exchanges enhanced by fluid circulation, dissolution–precipitation reactions that can result in isotopic heterogeneities at a very fine scale. However, as mentioned above, there is now compelling evidence that texturally and chemically-controlled *in situ* $^{40}\text{Ar}/^{39}\text{Ar}$ analyses of such rocks can provide significant data to decipher the succession of deformation episodes in tectonites. This is also due to the fact that for rocks deformed below 500 °C, it is now widely accepted that $^{40}\text{Ar}/^{39}\text{Ar}$ ages of synkinematic

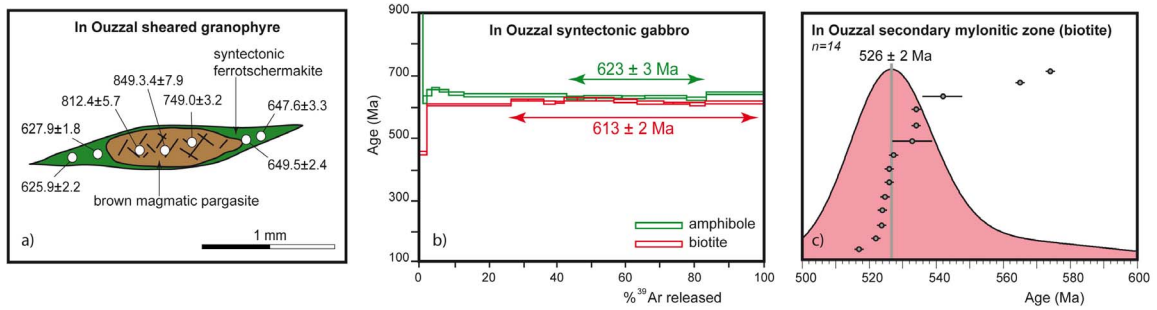


Figure 7. *In situ* and step-heating $^{40}\text{Ar}/^{39}\text{Ar}$ data from the In Ouzzal shear zone. (a) *In situ* dates on prekinematic and synkinematic amphibole from a sheared granophyre; (b) age spectra of amphibole and biotite from a syntectonic gabbro; (c) *in situ* date distribution (Kernel density plot) on fine biotites from a narrow mylonitic band [Ferkous and Monié, 2002].

minerals represent (re)-crystallization ages rather than cooling ages [e.g. Agard *et al.*, 2002, Augier *et al.*, 2005, Rolland *et al.*, 2008, Sanchez *et al.*, 2011, Di Vincenzo *et al.*, 2016, Villa *et al.*, 2014, Bosse and Villa, 2019]. However, the interpretation of *in situ* $^{40}\text{Ar}/^{39}\text{Ar}$ analyses in polydeformed rocks can be faced with different problems: the isotopic inheritance in relict phases that are not fully reset during shearing, the chemical complexity of newly formed minerals (zonation, mica interlayering) and their fine grain size, the presence of short circuit pathways for argon migration, the presence of excess argon trapped at the time of mineral crystallization or later, the late interaction with fluids. Below, we present some examples that highlight the relevance of *in situ* $^{40}\text{Ar}/^{39}\text{Ar}$ analyses compared to more conventional argon degassing modes for dating mid-upper crustal deformation in orogens.

2.3. Examples of *in situ* $^{40}\text{Ar}/^{39}\text{Ar}$ dating of shear zones

2.3.1. *In situ* $^{40}\text{Ar}/^{39}\text{Ar}$ dating of amphibole from shear zones

In crustal deformation zones, micas are the main target of *in situ* $^{40}\text{Ar}/^{39}\text{Ar}$ investigations because of their ability to accommodate strain constraints by different deformation mechanisms (kinking, gliding parallel to cleavage) and different (re-)crystallization processes in the presence of fluids. On rare occasions, shear zone amphiboles were dated by this technique and an example from the upper Neoproterozoic

shear zone of In Ouzzal in southern Algeria is given below [from Ferkous and Monié, 2002]. In south Algeria, the Hoggar shield belongs to a Neoproterozoic (800–600 Ma) orogenic belt that was juxtaposed to the Archean West African craton by large-scale N–S striking subvertical strike-slip shear zones under upper greenschist–amphibolite metamorphic conditions. The studied shear zone is a 3 km wide corridor made of protomylonites, mylonites and ultramylonites and contains abundant pre- to synkinematic igneous rocks, as well as syn- to postkinematic auriferous quartz veins. Amphibole from a prekinematic granophyre is of two types, brown magmatic porphyroclastic pargasite and blue-green ferrotschermakite in the pressure shadow of pargasite. *In situ* $^{40}\text{Ar}/^{39}\text{Ar}$ analyses (Figure 7a) provide dates between 749 and 849 Ma for the magmatic amphibole and between 626 and 650 Ma for the metamorphic one, consistent with the step-heating analyses of amphibole (623 Ma) and biotite (613 Ma) from a synkinematic granodiorite in the shear zone (Figure 7b). The estimated P – T conditions of shearing are about 0.4 GPa and 450–500 °C, suggesting that the dates of synkinematic ferrotschermakite can be interpreted as crystallization ages close to the peak of metamorphism related to the main episode of fault activity along the In Ouzzal shear zone, in agreement with the muscovite age of synkinematic gold-rich quartz veins (611 Ma). In this sample, the primary magmatic amphibole is partially reset and the date of 849 Ma can be taken as a minimum estimate for the age of granophyre emplacement and cooling. This large deformation corridor was locally reactivated about 100 Ma

later by a second episode of strike-slip tectonics as attested by *in situ* $^{40}\text{Ar}/^{39}\text{Ar}$ dating of fine grained biotite in a narrow ultramylonitic band (Figure 7c).

This study highlights (1) the interest of the laser microprobe approach to differentiate the ages of synkinematic amphibole from prekinematic amphibole, which is not always possible with the dating of mineral populations; (2) the common characteristic of faults to be weakness zones that can have a long term activity, and which can result in the coexistence of multiple generations of newly formed minerals during diachronous episodes of shearing.

2.3.2. *In situ* $^{40}\text{Ar}/^{39}\text{Ar}$ dating of white mica from shear zones

Three examples are presented in this section, the Oisans external massif (western Alps), and two massifs of the eastern Pyrenees, the Agly massif (North Pyrenean Zone) and the Cap de Creus massif (Axial Zone). All these massifs are made of a Variscan basement overprinted to various extent by Alpine deformations under greenschist to upper greenschist metamorphic conditions, resulting in a mixture of Variscan and Alpine mineral assemblages dominated by Variscan minerals in the weakly deformed rocks and sometimes vice-versa. For these massifs, there were few geochronological studies of the deformation zones themselves and debates persisted about the relative importance of pre-Alpine or Alpine deformation on the present structuration of these two belts. This is particularly true for the two Eastern Pyrenees massifs for which in the absence of systematic geochronological studies focused on shear zones, controversies still remain since several years on the age of their activity, varying by authors from the late Paleozoic to the Eocene.

In the Oisans massif, *in situ* $^{40}\text{Ar}/^{39}\text{Ar}$ studies were carried on different W-directed reverse shear zones that accommodate E–W shortening during the Alpine collision. The main goal of this study was to document the westward propagation of the deformation on variously strained samples and to evaluate the effect of mixture between partially or totally recrystallized Variscan muscovite and newly-formed synkinematic Alpine phengite in protomylonites, mylonites and phyllonites formed at temperature below 350 °C [Bellanger *et al.*, 2015]. EPMA analyses of white-micas yield two distinct end-members with very few

intermediate values. The first end-member corresponds to prekinematic muscovite clasts (Si = 3.15; Na = 0.06–0.08) and the second one to synkinematic phengite (Si = 3.2–3.4; Na = 0–0.02). *In situ* $^{40}\text{Ar}/^{39}\text{Ar}$ analyses were obtained on three samples selected over a single strain gradient of a major shear zone. The results are synthesized in Figure 8 which shows for each protomylonite, mylonite and phyllonite sample, the textural aspect of the dated rock section, the distribution of *in situ* dates on this section and the Kernel density plot for these $^{40}\text{Ar}/^{39}\text{Ar}$ ages.

In the less deformed sample containing discrete shear bands (protomylonite), *in situ* ages are scattered between 207 ± 5 Ma and 24 ± 2 Ma (Triassic to Miocene). Of the 29 dates, only 6 are younger than 34 Ma, the maximum age of Alpine deformations imposed by stratigraphic constraints. Interestingly, these dates come from small and low Cl/K (<0.01) phengites from the core of the shear bands. 12 analyses provide the oldest dates (>50 Ma) outside the shear bands and are correlated with relatively high Cl/K ratio (0.01–0.02). They correspond to partially recrystallized inherited muscovites with no peak age in the cumulative correlation plot, which indicates that Variscan muscovite experienced variable argon loss during Alpine thermotectonic overprint and interaction with Alpine fluids. The data do not enable to discount the possibility that an initial argon resetting may have occurred as early as the Permian or Triassic. The mylonite sample partially preserved its Variscan fabrics (high-temperature foliation) and is cut by a 3 mm-thick shear band where Alpine synkinematic recrystallizations are almost complete. In the shear band, phengite yields a range of *in situ* dates between 30 and 40 Ma with a peak age at about 32 Ma for the micas from the core of the shear band (12 of 30 analyses) while those from its inner edge are older than 34 Ma (red line on Figure 8). Outside the shear band, muscovite clasts yield older dates (48–129 Ma) with higher Cl/K ratios than phengite, as observed in the protomylonite. These relationships, only detectable by *in situ* analyses, indicate that synkinematic crystallization of phengite by dissolution–precipitation processes at the expense of K-bearing Variscan minerals (muscovite and feldspar) was more complete in the core of the shear band than at its edge and even more than in the host rock. In the phyllonite almost devoid of muscovite clasts, of the 29 dates of phengite

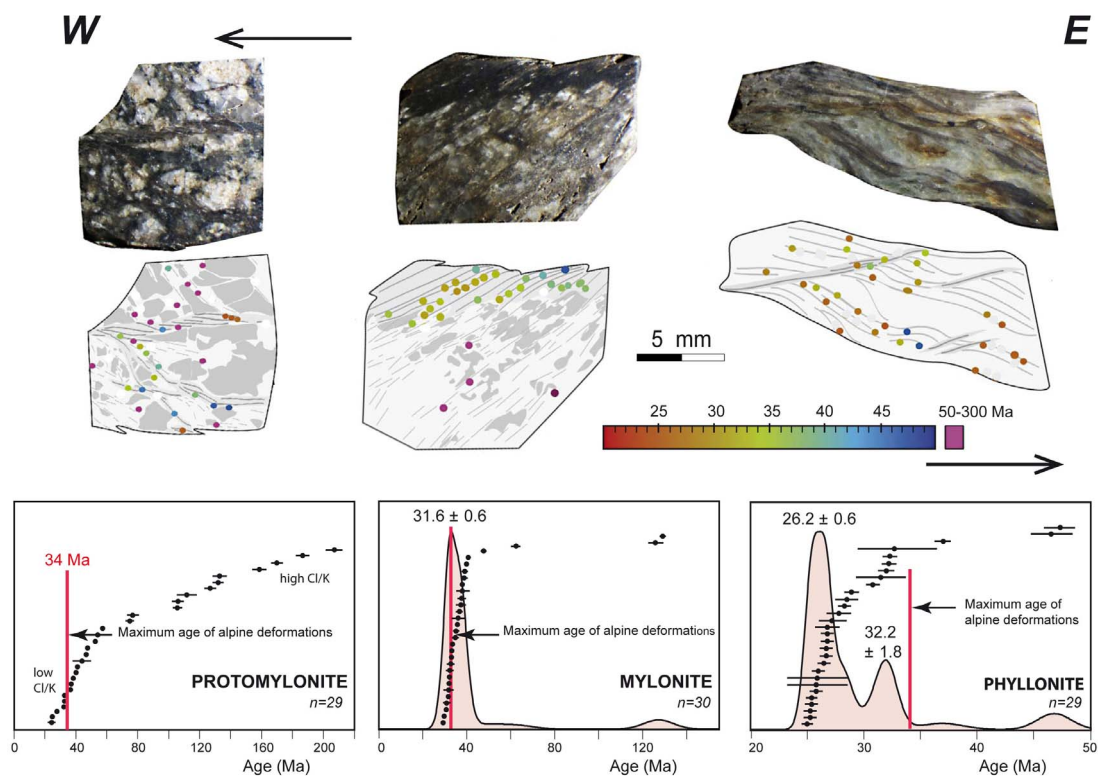


Figure 8. *In situ* $^{40}\text{Ar}/^{39}\text{Ar}$ analyses on three samples of Variscan gneiss showing, from left to right, an increase of Alpine deformation over a major shear zone of the Oisans massif. The red line corresponds to the maximum age of Alpine deformations imposed by stratigraphic constraints [modified from Bellanger *et al.*, 2015].

($\text{Cl}/\text{K} < 0.01$), only 3 are older than 34 Ma while the remaining dates define two peaks, a major peak at 26 Ma and a minor one at 32 Ma consistent with the peak date given by phengite in the mylonite. These *in situ* data are consistent with those provided by a previous step-heating study focused on ultramylonites that also highlighted some contamination by excess argon related to the presence of Ca-rich impurities in the dated mineral populations and limited argon loss possibly due to hydrothermal alteration [Simon-Labric *et al.*, 2009]. In our example, the correlation of *in situ* $^{40}\text{Ar}/^{39}\text{Ar}$ ages and deformation intensity within and between the three dated sections shows that the distribution of Alpine ages is primarily controlled by deformation textures. The data also show that the presence of Alpine ages in the three dated rock sections is correlated with the intensity of phengite blastesis, particularly important in high-strain zones along which fluids circulated. Consid-

ering that temperatures reached during the Alpine orogeny in the Oisans massif did not exceed 300–350 °C, it is very likely that the ages retained by newly-formed phengites represent true crystallization ages, provided that they evolved in a closed system, without being contaminated by excess (extraneous or inherited) argon. Phengite dates are distributed on two Oligocene peak ages that are interpreted to record the progressive localisation of deformation along the highly strained tectonites in the Oisans massif during E–W shortening [see Bellanger *et al.*, 2015, for a more complete discussion].

In the eastern Pyrenees, the mylonitic shear zones occurring in the Variscan basement at Cap de Creus have been the subject of detailed structural studies [e.g. Carreras *et al.*, 1977, 2010, Druguet *et al.*, 1997, 2009] and are generally attributed to the end of the Variscan orogeny. This assumption was recently challenged by a $^{40}\text{Ar}/^{39}\text{Ar}$

geochronological study that argues for a Jurassic age for these relatively low-temperature (~ 450 °C) shear zones, with possible Tertiary reactivation [Vissers *et al.*, 2016, 2020]. However, the significance of these ages remains largely uncertain due to the large grain size of the dated muscovite (180–250 μm) compared to the size of synkinematic micas (< 100 μm). Some new *in situ* and step-heating $^{40}\text{Ar}/^{39}\text{Ar}$ geochronological data are presented below that allow us to propose an Eocene age for the most obvious mylonitic deformation in the Cap de Creus massif [Monié *et al.*, 2018].

The first sample is an ultramylonitic Variscan pegmatite [299 Ma U–Pb zircon age, van Lichtervelde *et al.*, 2017] that was collected in the core of a 2 m wide NW–SE dextral shear zone in the Cap de Creus peninsula, close to the locality sampled by Vissers *et al.* [2016]. The mica population contains some rare muscovite clasts but is dominated by fine-grained synkinematic phengitic muscovite ($\text{Si} = 3.1\text{--}3.2$) formed at the expense of Variscan muscovite by fluid-assisted dissolution–precipitation mechanisms (Figure 9a).

This population was studied using stepwise and *in situ* heating experiments on two size fractions and on a thick section made perpendicular to the foliation and parallel to the lineation, respectively. The age spectrum of a single muscovite clast (300–400 μm) shows a saddle-shaped pattern with dates of 101–133 Ma while about 30 grains of synkinematic phengitic muscovite (80–100 μm) give a plateau-like date of 42 ± 1 Ma (Figure 9b). *In situ* analyses of micas along the foliation plane yield dates ranging from 43 Ma to 83 Ma with a peak at 45 Ma in the cumulative probability diagram (Figure 9c). This peak age validates the ~ 42 Ma plateau-like date of the fine-grained mica fraction as no value below 42 Ma was obtained. Older *in situ* dates confirm that small relics of Variscan muscovite, still containing some inherited argon, are present along the foliation, but are not optically distinguishable from synkinematic micas. All these new dates are much younger than the Jurassic ages (159–175 Ma) reported by Vissers *et al.* [2016] and point to an Eocene age for the main ductile activity of shear zones in the Cap de Creus peninsula. They also show how critical the choice of samples and minerals to date is in mylonites (strain intensity, grain size, mineral habit...) and how useful the *in situ* approach is to identify the different mica

generations compared to the other methods of argon extraction. This is particularly true for the total melting approach which is biased by the selection of the largest mica grains in the sheared rocks, which is not the case for the fabric-preserving *in situ* approach that allows to target micas that differ in size, chemistry or textural habit.

This is confirmed by the study of mylonitic shear zones in the Roses granodiorite, 15 km southwest of the previous shear zone. This Variscan magmatic body [291 Ma U–Pb zircon age, Druguet *et al.*, 2014] is affected by zones of heterogeneous and localised mylonitic deformation resulting from the coexistence of brittle and ductile deformation mechanisms and fluid-induced mineralogical softening reactions. In the most deformed facies, these reactions induce a complete replacement of plagioclase by epidote \pm phengite, and magmatic biotite by more magnesian metamorphic biotite and white mica (Figure 10a) at a temperature of 450–500 °C.

In situ $^{40}\text{Ar}/^{39}\text{Ar}$ dates were obtained on two protomylonitic and mylonitic samples, both showing an increasing gradient of deformation and metamorphic recrystallization. In the protomylonite, *in situ* biotite dates range from 69 Ma to 47 Ma from the least to the most deformed domains, with a peak age of about 49 Ma for the more sheared zone (Figure 10b). In the mylonite, biotite from the least deformed portion yields a range of values between 41.5 Ma and 47.5 Ma with a peak date of 44 Ma for newly crystallized biotite. In the shear band with abundant synkinematic phengite, *in situ* $^{40}\text{Ar}/^{39}\text{Ar}$ dates are mainly between 39 Ma and 42 Ma with a peak at ~ 40 Ma (Figure 10c). These texturally and chemically controlled *in situ* $^{40}\text{Ar}/^{39}\text{Ar}$ analyses indicate that deformation and associated metamorphic recrystallizations play a prominent role in the distribution of dates at the scale of a centimeter section, with younger dates in the most deformed domains. Furthermore, the preservation of these deformation–recrystallization–chemistry–age relationships again suggests that the $^{40}\text{Ar}/^{39}\text{Ar}$ dates recorded by biotite and phengite in these mylonites should be considered as crystallization ages rather than cooling ages. In the mylonite, the 4 Myr time lag between the crystallization of metamorphic biotite in the host rock matrix and the crystallization of phengite in the shear band may represent the time required to switch from a diffuse to a localized deformation regime. These

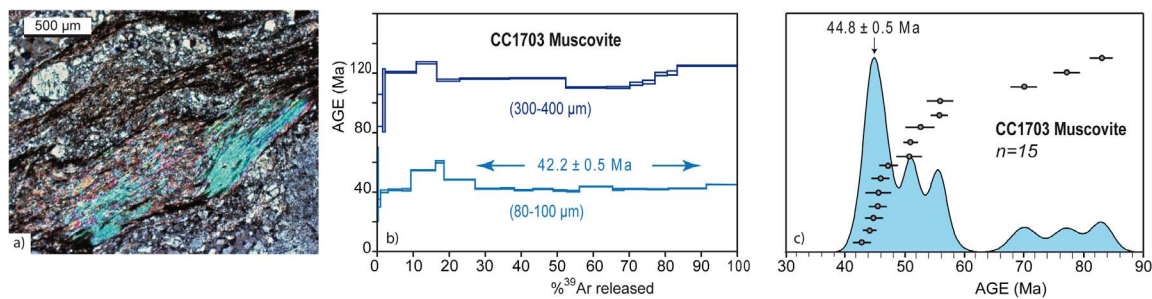


Figure 9. Ultramylonitic pegmatite from the Cap de Creus peninsula; (a) thin section with a scarce sheared and recrystallized clast of muscovite in a fine matrix of quartz, albite and phengitic muscovite; (b) age spectra on two granulometric fractions representative of the two mica populations; (c) distribution of *in situ* $^{40}\text{Ar}/^{39}\text{Ar}$ dates obtained on a thick section [Monié *et al.*, 2018].

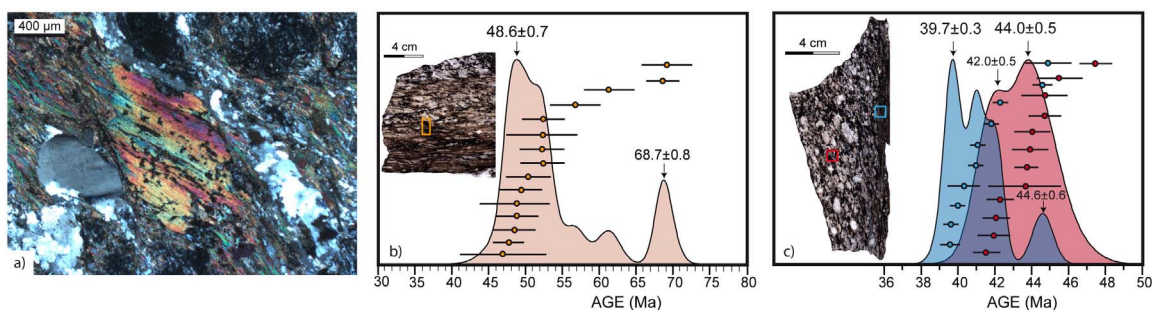


Figure 10. Sheared granodiorite from the Roses massif; (a) thin section showing the coexistence of prekinematic magmatic and synkinematic metamorphic biotite; (b) distribution of *in situ* $^{40}\text{Ar}/^{39}\text{Ar}$ dates across a gradient of deformation showing some biotite relics; (c) distribution of *in situ* $^{40}\text{Ar}/^{39}\text{Ar}$ dates within two sections of mylonitic granodiorite (red square) and shear band (blue square) [Monié *et al.*, 2018].

data suggest an Eocene age for the mylonitisation of the Roses granodiorite, in agreement with the data reported above in the Cap de Creus peninsula. On a regional scale, it is proposed that these NW–SE striking mylonitic strike-slip structures accommodated the end of the Pyrenean compression [e.g. Teixell *et al.*, 2018, Ternois *et al.*, 2019].

Recently, new Th–U/Pb and $^{40}\text{Ar}/^{39}\text{Ar}$ geochronological data were obtained in the Agly massif [Aumar *et al.*, 2022], which has long been the subject of debate as to the influence of Cretaceous deformations on its architecture. The study focused on the Lower Gneiss Unit that shows a highly ductile extensional deformation with a NNE–SSW oriented stretching lineation that is also found in the Mesozoic sedimentary series to the north. In the basement gneisses, the original high-temperature Variscan deformation was overprinted by this new extensional deformation that

evolved continuously from a ductile regime at relatively high temperature ($\geq 500^\circ\text{C}$) to a brittle regime at a very low temperature ($150/200^\circ\text{C}$). Synkinematic minerals located within shear bands provided consistent Th–U/Pb monazite and $^{40}\text{Ar}/^{39}\text{Ar}$ mica dates with a 94–127 Ma age bracket interpreted as dating mylonitic deformation during the Cretaceous rifting episode that preceded the building of the chain. An example of stepwise heating and *in situ* $^{40}\text{Ar}/^{39}\text{Ar}$ data is shown in Figure 11.

Several samples of proto- to ultramylonites (Figure 11a) were collected throughout the massif and regardless of the degree of mylonitisation, muscovite and biotite yield a cluster of well-defined plateau ages of 104–105 Ma (Figure 11b). These ages were obtained on mica clasts preserved in the mylonitic matrix and the lack of intra- and inter-sample age gradient suggests that the dated micas

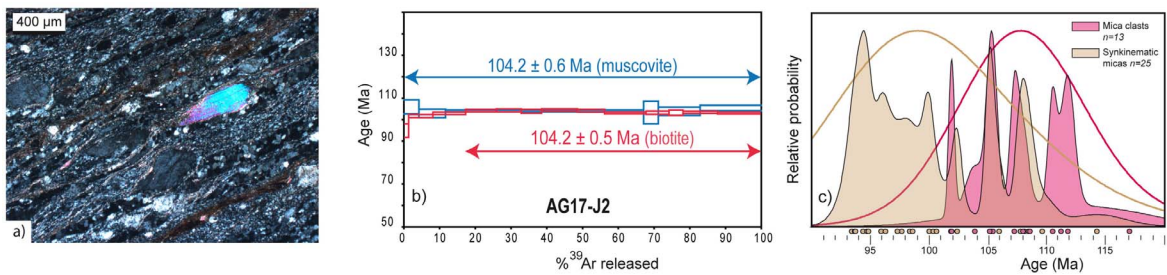


Figure 11. (a) Mylonitic leucogranite [291 Ma U–Pb monazite age, Vanandois *et al.*, 2022] with a magmatic muscovite clast in a matrix of synkinematic fine-grained biotite and muscovite; (b) age spectra of muscovite and biotite clasts from a protomylonitic gneiss; (c) distribution of *in situ* $^{40}\text{Ar}/^{39}\text{Ar}$ dates obtained on four thick rock sections of mylonites. A Kernel density bell-shaped curve has been drawn for each mica population [Aumar *et al.*, 2022].

experienced a full reset of their K–Ar chronometer, which is supported by the U–Th/Pb age of 104–127 Ma for synkinematic monazite in the same samples [see Aumar *et al.*, 2022]. *In situ* $^{40}\text{Ar}/^{39}\text{Ar}$ analyses were carried on 4 thick sections of proto-ultra-mylonites and the distribution of ages obtained on both large prekinematic mica clasts and tiny synkinematic micas is shown on Figure 11c. The main observation is that texturally earlier micas show older dates than newly crystallized micas in the foliation, mainly between 102 and 112 Ma for the clasts ($n = 12$) and between 94 and 102 Ma ($n = 17$) for the new micas. This age range (112–94 Ma) is interpreted to cover a large part of the ductile deformation in the Agly massif. Lastly, it can also be noted that these *in situ* $^{40}\text{Ar}/^{39}\text{Ar}$ analyses provide no evidence for the significant presence of an inherited Variscan argon component in the dated micas. These results from the Agly massif are contrasting with those of the Oisans and Cap de Creus massifs for which some micas in the high strain zones still contain inherited argon (Figures 8b,c and 9c). There are several explanations for the results obtained in the Agly massif: a higher temperature (≥ 500 °C) at the beginning of the deformation supported by the micro-fabric of quartz, feldspar and garnet in the mylonites, a more penetrative and long-lived mylonitic deformation (~ 40 myrs) in an extensional tectonic context, more extensive fluid-rock interactions highlighted by the widespread Cretaceous hydrothermal activity in the Northern Pyrenees [e.g. Boutin *et al.*, 2016] and attested by a notable contribution of chlorine-derived ^{38}Ar in some $^{40}\text{Ar}/^{39}\text{Ar}$ analyses.

3. $^{40}\text{Ar}/^{39}\text{Ar}$ Ar geochronology of brittle deformation

Classically, the dating of brittle deformation is indirectly inferred from the dating of geological units that predate and postdate the fault activity. More recently, with the development of low temperature thermochronometric tools, fault motion is also inferred from differential thermal histories of the foot-wall and the hangingwall rocks [Malusà and Fitzgerald, 2019, and references therein]. Rapid cooling or exhumation of wall rocks are often explained by fault motion responsible for isotherm advection. However direct $^{40}\text{Ar}/^{39}\text{Ar}$ (or K–Ar) dating of fault motion is possible even in the low temperature upper crust corresponding to the partial annealing zone of apatite fission tracks (Figure 12). $^{40}\text{Ar}/^{39}\text{Ar}$ (K–Ar) dating method has been successfully applied on fault gouges using synkinematic/authigenic clay minerals that form during the activity of shallow crustal faults from above the ductile–brittle transition [e.g. van der Pluijm *et al.*, 2001], i.e. in a range of temperature between ~ 300 °C, corresponding to the muscovite–illite transition, to ~ 140 – 60 °C corresponding to the temperature range of illite-rich illite–smectite (I/S) interstratified mineral formation [Haines and van der Pluijm, 2012]. The $^{40}\text{Ar}/^{39}\text{Ar}$ (K–Ar) dating method is very useful to provide direct constraints on the timing of shallow crust faulting but also it can yield information regarding the thermal history of the fault-zone rocks. Note that during the last decade, the U–Pb geochronology of calcite has been widely developed to address the timing of brittle faulting

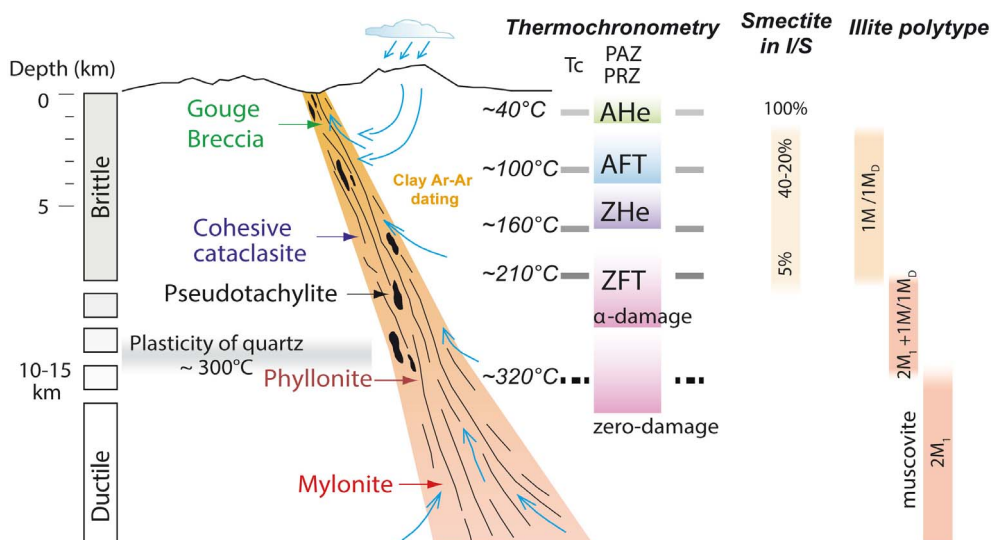


Figure 12. Fault-rock types and evolution of related deformation mechanisms with depth. Brittle deformation corresponds to the temperature range of low temperature thermochronometers: Zircon Fission Tracks (ZFT), Zircon (U–Th)/He (ZHe), Apatite Fission Tracks (AFT) and Apatite (U–Th)/He (AHe). Closure temperature of each thermochronometric system is reported; PAZ: partial annealing zone; PRZ: partial retention zone [modified after Malusà and Fitzgerald, 2019].

and fracturing [Roberts and Holdsworth, 2022, for a review].

3.1. Some methodological aspects

Synkinematic/authigenic clay minerals are characterized by their micron size (2 to 0.2 μm size fractions are commonly analyzed, and sometimes down to the 0.05 or up to 20 μm size fractions) that favors a ^{39}Ar recoil effect during irradiation [Reuter and Dallmeyer, 1987, Onstott *et al.*, 1995]. The distance of ^{39}Ar recoil during irradiation was estimated to be a mean of 0.08 μm [Onstott *et al.*, 1995], which has significant effects on small crystallites. One must keep in mind that ^{39}Ar recoil distance is also a function of fast neutron energy in the irradiation facility, and therefore the amount of argon loss is also dependent on this energy. Although the fraction of ^{39}Ar lost by recoil effect generally increases with decreasing grain size, Dong *et al.* [1995] also showed that the amount of ^{39}Ar recoil is rather dependent on the degree of crystallization of clay particles. During irradiation, the amount of ^{39}Ar loss can reach 30% of the total amount of ^{39}Ar produced which results in

apparent $^{40}\text{Ar}/^{39}\text{Ar}$ ages older than K–Ar ages. This limitation favored K–Ar dating of clay minerals for a long time [Clauer *et al.*, 2012, Clauer, 2013], despite this method presents two main drawbacks: argon and potassium are measured on separated clay aliquots, and it does not permit to discriminate illite-rich mineral generations resulting from multistage crystallization. In the 90s, a sample encapsulation technique was developed in order to measure the ^{39}Ar lost by clay particles during irradiation and to correct $^{40}\text{Ar}/^{39}\text{Ar}$ ages [Foland *et al.*, 1992, Dong *et al.*, 1995, Onstott *et al.*, 1995]. Each sample (~1 mg) is encapsulated and sealed under vacuum within a quartz tube that traps the ^{39}Ar released during neutron irradiation. The ^{39}Ar loss can then be measured by breaking or laser drilling the quartz tube under vacuum in the sample chamber to correct the bulk $^{40}\text{Ar}/^{39}\text{Ar}$ age obtained by classical step-heating $^{40}\text{Ar}/^{39}\text{Ar}$ method. Dong *et al.* [1995] defined a “retention age” (RA) corresponding to the $^{40}\text{Ar}/^{39}\text{Ar}$ total age that omits the fraction of ^{39}Ar lost during irradiation and a “total gas age” (TGA) including ^{39}Ar recoil. Dong *et al.* [1995] also showed that the fraction of ^{39}Ar lost by recoil is a linear function of illite crystallinity. For thick

crystallite, i.e. >50 nm, the “retention age” and the “total gas age” are close or identical. For thin crystallites, i.e. <10–15 nm, the “total gas age” can be considered as the best estimate of the crystallization age. For crystallites with intermediate thickness, crystallization ages fall between the “retention age” and the “total gas age”. Fitz-Diaz *et al.* [2016] proposed to correct $^{40}\text{Ar}/^{39}\text{Ar}$ ages by taking into account the average illite crystallite thickness (ICT)—considered as the number of TOT layer and related to illite crystallinity—and the corresponding recoiled ^{39}Ar . This correction is particularly useful for samples containing authigenic illite with typical ICT between 10 and 50 nm.

At last, Lin *et al.* [2000] showed that the recoil effect is also influenced by the incident angle of the neutron flux with the *c*-axis of clay particles. A soft compaction of clay particles before *in vacuo* sealing is thus recommended to significantly reduce the recoil effect [Dong *et al.*, 1995, Clauer *et al.*, 2012]. During encapsulation there is a risk to heat the samples while sealing the quartz tube. The sealing is realized with a gas torch and in order to prevent heating the sample, the base of the tube containing the sample is placed either in iced water [Clauer *et al.*, 2012, Hall, 2015] or in a metallic holder cooled with liquid nitrogen. Clauer *et al.* [2012] questioned the accuracy of $^{40}\text{Ar}/^{39}\text{Ar}$ ages compared to K–Ar ages and argued that the lack of standardization of encapsulation processes may be a source of bias in $^{40}\text{Ar}/^{39}\text{Ar}$ dating of clay minerals and this should be addressed. To the whole, the encapsulation systems have been constantly improved and are now used routinely in several laboratories. For example, at Géosciences Montpellier, we developed an encapsulation system allowing encapsulating clay samples under very low vacuum before their irradiation, i.e. vacuum of 10^{-9} torr is currently reached (Figure 13) [Abd Elmola *et al.*, 2018, Münch *et al.*, 2021]. Reproducibility tests of $^{40}\text{Ar}/^{39}\text{Ar}$ ages on different clay aliquots and comparisons with K–Ar ages show the reliability of this encapsulation technique, with smaller error margins than for the K–Ar method.

A second issue with $^{40}\text{Ar}/^{39}\text{Ar}$ (or K–Ar) dating of clay minerals from gouges is related to tectonic processes occurring within shallow crust faults: fragmentation of host rocks followed by grain-size reduction and authigenesis of clay minerals, resulting in a mixture of inherited/detrital and authi-

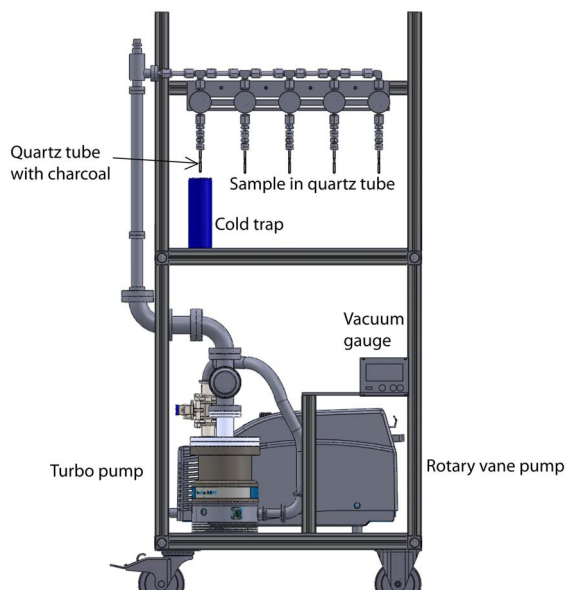


Figure 13. Sketch of the encapsulation device developed at the Géosciences Montpellier noble gas laboratory. The quartz tube containing the charcoal is immersed in liquid nitrogen to improve the vacuum in the encapsulation line.

genic/synkinematic minerals and in the measurement of a mixed age. Depending on the lithology of the wall rock, authigenesis will correspond either to the illitisation of interstratified illite/smectite minerals present in sedimentary host rocks or to the neocrystallization of discrete illite in the case of metamorphic or magmatic host rocks, devoid of clay minerals [Haines and van der Pluijm, 2008] (Figure 14). From the ductile/brittle transition, i.e. at temperature around 300 °C, newly formed illite is mainly of 2M₁ polytype (polytypism is a variety of polymorphism common in layered minerals) with minor 1M/1M_d polytype and their relative proportion are inverted with decreasing temperatures (Figure 14). Below ~200 °C, 1M/1M_d polytype is the only newly formed polytype and with decreasing temperatures the proportion of illite in I/S minerals decreases and ordering of illite layers within I/S also decreases (Figure 14). Thus at shallow depth, the proportion of inherited/detrital and newly formed phases can be resolved through quantitative X-ray diffraction analysis of different clay size fractions.

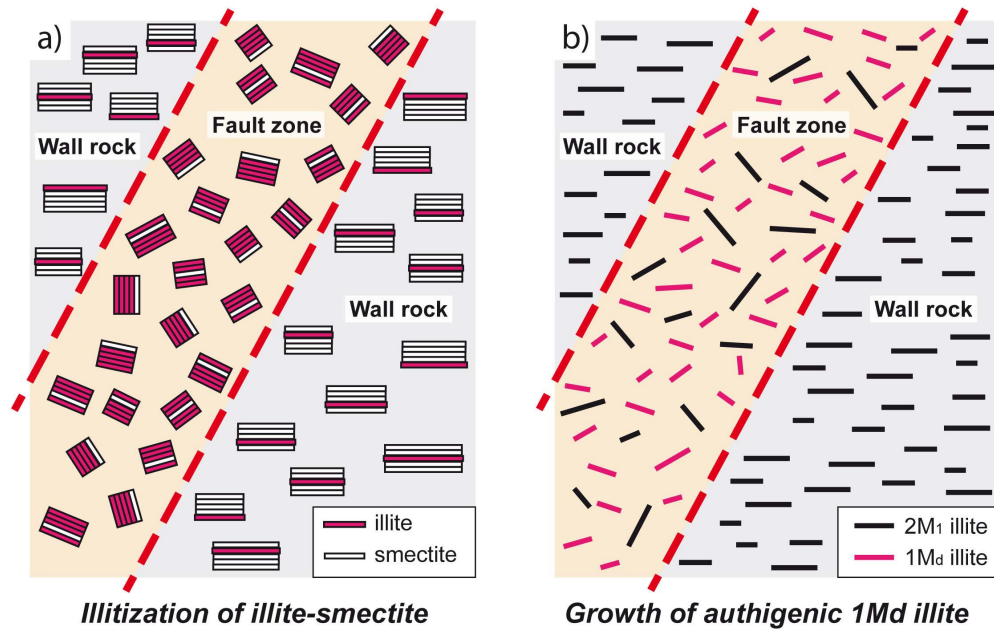


Figure 14. Mineral transformations within fault gouges to form illite-rich clay minerals suitable for $^{40}\text{Ar}/^{39}\text{Ar}$ (K/Ar) dating [modified after Haines and van der Pluijm, 2008]. (A) Illitization of illite–smectite (I/S) interstratified minerals present within the wall rock; this process results in higher contents of I/S minerals within the gouge than in the wall rock. (B) Growth of authigenic discrete $1M_d$ illite in fault gouges; this process results in a mixture of authigenic/synkinematic $1M_d$ illite and inherited/detrital $2M_1$ illite (= muscovite) from the wall rock.

For less shallow crustal faults, but still above the brittle–ductile transition, the problem of dating a mixture of inherited/detrital and authigenic/synkinematic illite type minerals is much more difficult to solve. Indeed, with X-ray diffraction techniques, muscovite forming at temperatures above 300 °C is undistinguishable from $2M_1$ illite polytype forming at temperatures down to ~200 °C (Figure 12). As a consequence, if muscovite is present within host rocks both authigenic/synkinematic and inherited/detrital $2M_1$ polytypes are mixed within the gouge rocks and their relative proportion cannot be estimated. At temperatures near 200 °C, $1M$ polytype authigenesis can also occur together with $2M_1$ but the proportion of detrital/authigenic can still not be estimated.

Like for $^{40}\text{Ar}/^{39}\text{Ar}$ dating of ductile deformation, a very thorough and precise mineralogical study of gouge samples must be conducted before dating them. In the case of clay minerals, this mineralogical study requires X-ray diffraction techniques on both

oriented and non-oriented powders in order to determine the mineralogy and quantify the proportion of different mineralogical phases. Scanning and transmission electron microscope studies are also necessary to determine the mineralogy of clay minerals and in some case their chemistry that can also be analyzed by electron microprobe but only for well-crystallized coarse clay minerals.

3.2. Age interpretation

$^{40}\text{Ar}/^{39}\text{Ar}$ age spectra obtained on encapsulated clay minerals differ from classical age spectra of magmatic or metamorphic minerals due to ^{39}Ar recoil effect during irradiation [Dong *et al.*, 1995, Hall *et al.*, 1997, 2000] but also to complex mixture of minerals with different age, polytype and crystallinity, without mentioning the possibility that the dated fractions may contain other types of potassium-rich minerals than phyllosilicates. In classical $^{40}\text{Ar}/^{39}\text{Ar}$ studies, samples have a size above 50 μm in order to

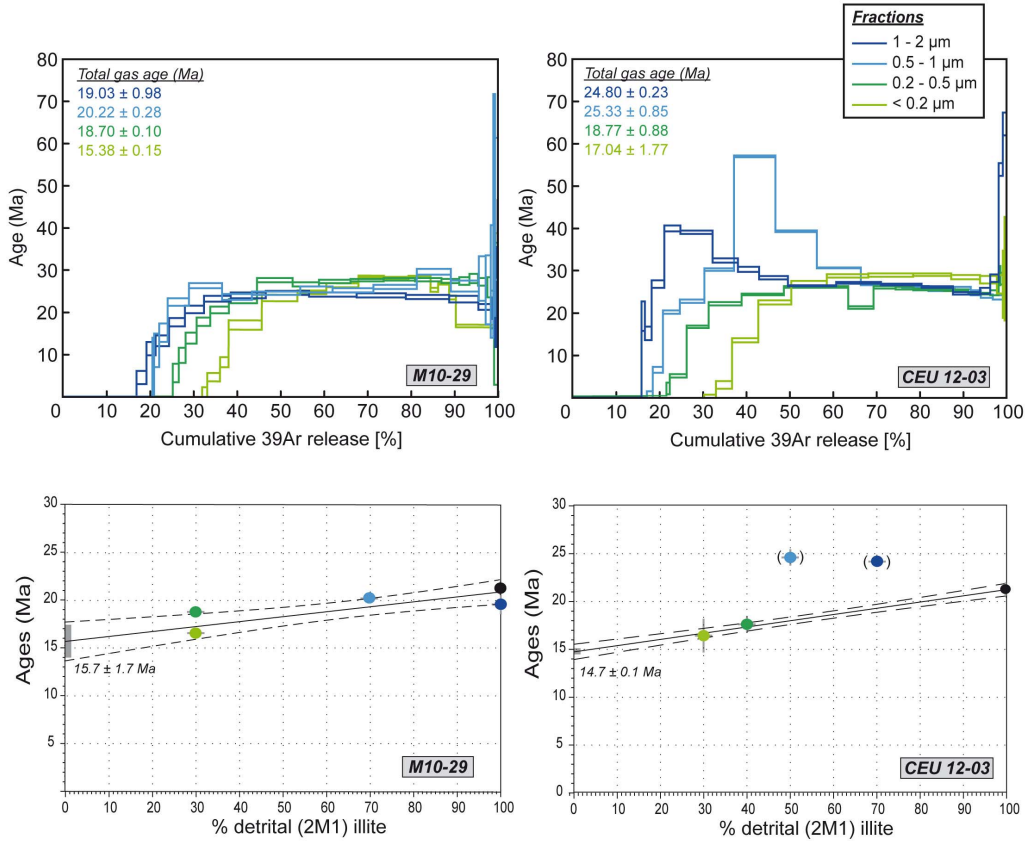


Figure 15. Examples of $^{40}\text{Ar}/^{39}\text{Ar}$ illite step-heating age spectra for vacuum-encapsulated clay gouge size fractions and illite age analysis plots [Pevear, 1999, van der Pluijm *et al.*, 2001] of $^{40}\text{Ar}/^{39}\text{Ar}$ illite TGA's vs. % $2M_1$ (detrital illite) of different clay-size fractions of two samples from late shallow crustal faults occurring within metamorphic units of the Rif chain [modified after Münch *et al.*, 2021]. (A) sample M10-29 showing classical spectra for all fractions and the corresponding illite age analysis plot. (B) Sample CEU12-03 showing complex spectra for two coarse fractions with low temperature staircase steps largely overshooting the “total gas” and “retention” ages as well as the age of muscovite from host rocks; the TGA's of corresponding fractions have been removed from illite age analysis (dots between brackets). On illite age analysis plots, the black dot on the right axis corresponds to the mean age of muscovite within the metamorphic host rocks.

avoid recoil induced ^{39}Ar loss and hopefully yield spectra with a plateau comprising more than 50% of total ^{39}Ar released and at least 3 steps. An illite spectrum shows different features: (1) a first zero age step corresponding to the recoil gas fraction, (2) staircase steps with increasing apparent ages from near zero at low temperature (3) a more or less hump-shaped age pattern with apparent ages that exceed the “retention age” and sometimes an age drop at highest temperatures (Figure 15A). This third part

of the spectrum sometimes looks like a seemingly good plateau but should be interpreted with great caution and as providing a meaningless intermediate age as in the case of hump-shaped spectra obtained for mixtures of two mica generations [Wijbrans and McDougall, 1986]. To estimate the age of a fault gouge motion, only the TGA's, eventually corrected for an ICT factor, of the different clay size fractions with well-identified polytype proportions must be used. Usually, TGA's decreases with grain size

and with the relative proportion of inherited/detrital and newly formed/synkinematic minerals of a given polytype. By plotting TGA's against the percentage of detrital polytype, the age of the pure authigenic phase can be determined with the ordinate intercept (0% of detrital component) of the best fitting line. This is the so-called "Illite Age Analysis" of Pevear [1999] and van der Pluijm *et al.* [2001] that has been applied on numerous shallow crust faults in various tectonic settings [e.g. Duvall *et al.*, 2011, Haines and van der Pluijm, 2008, 2010, 2012, Münch *et al.*, 2021, Ring *et al.*, 2017, Zwingmann *et al.*, 2010a,b; Figure 15A]. The ages calculated reflect the most recent period of activity of the faults along their exposure.

However, Solum *et al.* [2005] demonstrated that the illite age intercept calculated using the illite age analysis also varies from the fault core to the damage zone of a single fault, as a function of the intensity of the deformation and the proportion of authigenic illite. This result highlights that a thorough structural study of the fault zone that is to be dated is crucial and that samples selected for illite dating must come from the most deformed part of the fault. As authigenic illite or I/S growth in fault gouge occurs in a well constrained temperature range, it is important to combine fault gouge dating with thermochronological study of host rocks that constrains their cooling history. Low-temperature thermochronometric studies often emphasize one or more tectonic phases as the cause of accelerated exhumation and highlight the role of major faults. The combined use of thermochronometric tools and fault gouge dating allows the age of fault activity to be better constrained [Duvall *et al.*, 2011, Münch *et al.*, 2021, Milesi *et al.*, 2022, Parry *et al.*, 2001, Tagami, 2012].

In some cases, the $^{40}\text{Ar}/^{39}\text{Ar}$ age spectra of illite are more complex and the illite age analysis is not so straightforward. For example, some spectra from coarse fractions of gouge samples exhibit rather a saddle shape for the high temperature steps, i.e. after the staircase increase of apparent ages from zero, and in some cases the "total gas age" of these fractions has even been found older than the mean age of muscovite from the metamorphic host rocks [Münch *et al.*, 2021] (Figure 15B). The shape of the spectra may be interpreted in terms of excess of radiogenic ^{40}Ar [McDougall and Harrison, 1999] that probably originates from inherited minerals because

these spectra were only obtained for coarser fractions in which the proportion of inherited/detrital muscovite is higher. On the other hand, ^{40}Ar in excess could also have been incorporated during the growth of authigenic illites from fluids circulating within the fault [e.g. Roques *et al.*, 2020]. As the shape of the spectra allows detecting such excess of radiogenic ^{40}Ar , it must be considered before integrating the "total gas age" of each fraction in an illite age analysis. In some cases, with particularly complex shape of spectra, this can result in the rejection from the illite age analysis of the TGA(s) of the fraction(s) exhibiting such excess ^{40}Ar (Figure 15B).

In order to better interpret the $^{40}\text{Ar}/^{39}\text{Ar}$ age spectrum of authigenic illites, Clauer *et al.* [2012] applied a correction of ^{39}Ar recoil on step-heating experiments by distributing the recoiled ^{39}Ar on each step in proportion to its representative percentage on the retention age spectrum. The goal was to reconstruct an original spectrum, not altered by the ^{39}Ar recoil loss during the sample irradiation, which can be interpreted using the plateau age definition. The recoil-corrected spectrum of Clauer *et al.* [2012] is still similar to the spectra obtained from mixtures from which these authors defined one or two "limited plateaus", not necessarily corresponding to 3 concordant and consecutive steps. Clauer *et al.* [2012] claim that the "limited plateaus" represent different ^{39}Ar reservoirs and several illite generations for which they calculate a corrected age. Even if we agree that the complex spectra can reflect the mixture of several illite generations, other processes (fluid interaction, excess argon, mixture with other clay minerals or K-bearing inherited phases) can also lead to complex spectra. Above all, the correction applied is rather basic and the calculation of plateau ages for the different illite generations on a single spectrum is highly questionable. According to Fitz-Diaz *et al.* [2016] an age interpretation based on $^{40}\text{Ar}/^{39}\text{Ar}$ plateau ages is meaningless for most fine-grained clays because the grain size highly influences the shape of the spectra. However, the shape of the age spectra of different clay-size fractions from a single sample is obviously useful to depict the sample crystallization history in terms of mixture, excess ^{40}Ar incorporation and is a crucial point to take into consideration before performing an illite age analysis of a fault gouge. This is a huge advantage of the step-heating $^{40}\text{Ar}/^{39}\text{Ar}$ method compared to the

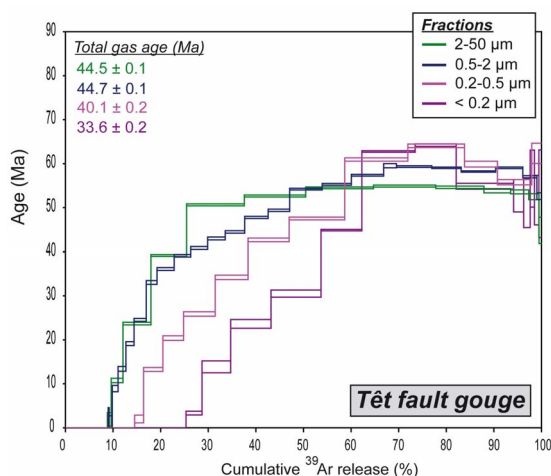


Figure 16. Examples of $^{40}\text{Ar}/^{39}\text{Ar}$ illite step-heating age spectra for vacuum-encapsulated clay gouge size fractions mainly constituted of $2M_1$ polytype (1M polytype is solely present in the $<0.2\ \mu\text{m}$ fraction) from the Têt fault in Eastern Pyrénées [Milesi, 2020].

complementary K–Ar method that cannot provide such information.

More complex cases come from the deeper brittle fault zones that were active at temperatures comprised between ~ 200 and $\sim 300\ ^\circ\text{C}$ (Figure 16). There, $^{40}\text{Ar}/^{39}\text{Ar}$ (K–Ar) ages decrease with decreasing clay-size fraction, illite crystallinity and increasing ^{39}Ar recoil loss [Milesi, 2020]. The illite age analysis cannot be applied because inherited and neo-formed illites are $2M_1$ polytype and the age of the finest fraction can only be considered as a maximum age as it is frequently a mixture of mainly $2M_1$ with minor 1M polytype. The age of coarse size fraction is potentially also a mixed age but the proportion of detrital muscovite and authigenic illite cannot be determined. However, the shape of the spectra can help to resolve if there is a mixture or not. The age of the medium size fraction may either represent a mixed age with a higher proportion of authigenic $2M_1$ illite or a cooling age of the same mixture as in the coarse fractions. This issue can be even more complicated if the host rock is detrital and was deeply buried at equivalent temperatures, between 200 and $300\ ^\circ\text{C}$, before faulting. In this case, the gouge can contain a complex mixture of detrital muscovite, $2M_1$ illite formed in anchizonal con-

ditions during burial and authigenic/synkinematic $2M_1$ illite. The age of fault motion is then very difficult to resolve and in such a case the stratigraphic age of host rocks as well as their clay mineralogy and the regional geological constraints have to be considered in order to correctly interpret the age of fault motion [Solum *et al.*, 2005, Abd Elmola *et al.*, 2022].

4. Pseudotachylytes

The long-term activity of faults is marked by a succession of events that are difficult to decipher precisely in a continuous way, particularly in the seismogenic upper crust. Among the various fault rocks, pseudotachylytes are witnesses of frictional flash melting associated with high-velocity co-seismic ruptures most often in the shallow and brittle domains of the lithosphere. They occur as glassy veins of variable thickness and are frequently associated with cataclasites and ultra-cataclasites, resulting in a complex, frequently asymmetric, zonation of the veins. Their melt origin is supported by the presence of a glassy material and different microstructures such as microlites, spherulites, vesicles, flow structures, vein injections, and sulfide droplets that are decisive criteria to differentiate them from crush-origin pseudotachylytes [Li *et al.*, 2022]. Because of the high cooling rates implied by their rapid solidification and their high potassium content, pseudotachylytes represent prime targets to date co-seismic displacement by the $^{40}\text{Ar}/^{39}\text{Ar}$ method [e.g. Kelley *et al.*, 1997, Sherlock and Hetzel, 2001, Müller *et al.*, 2002, Di Vincenzo *et al.*, 2004, Souquière *et al.*, 2011, Menant *et al.*, 2018, Mittempergher *et al.*, 2022]. Step-heating analysis of pseudotachylyte fragments has produced variously successful results due to the very heterogeneous character of the veins (abundant host rock clasts, partial devitrification, inclusions . . .) and the often polyphased history of fault zones [e.g. Torgersen *et al.*, 2022]. The use of the *in situ* laser probe $^{40}\text{Ar}/^{39}\text{Ar}$ dating method has partially overcome some of these drawbacks by focusing the analyses on particular zones rich in molten glass and poor in clasts, such as the vein margins or the injection veins. Below (Figure 17) are some examples showing some characteristics of pseudotachylytes and some data obtained in the western Alps (Ivrea zone, Dent Blanche) using both step-heating and *in situ* $^{40}\text{Ar}/^{39}\text{Ar}$ analyses.

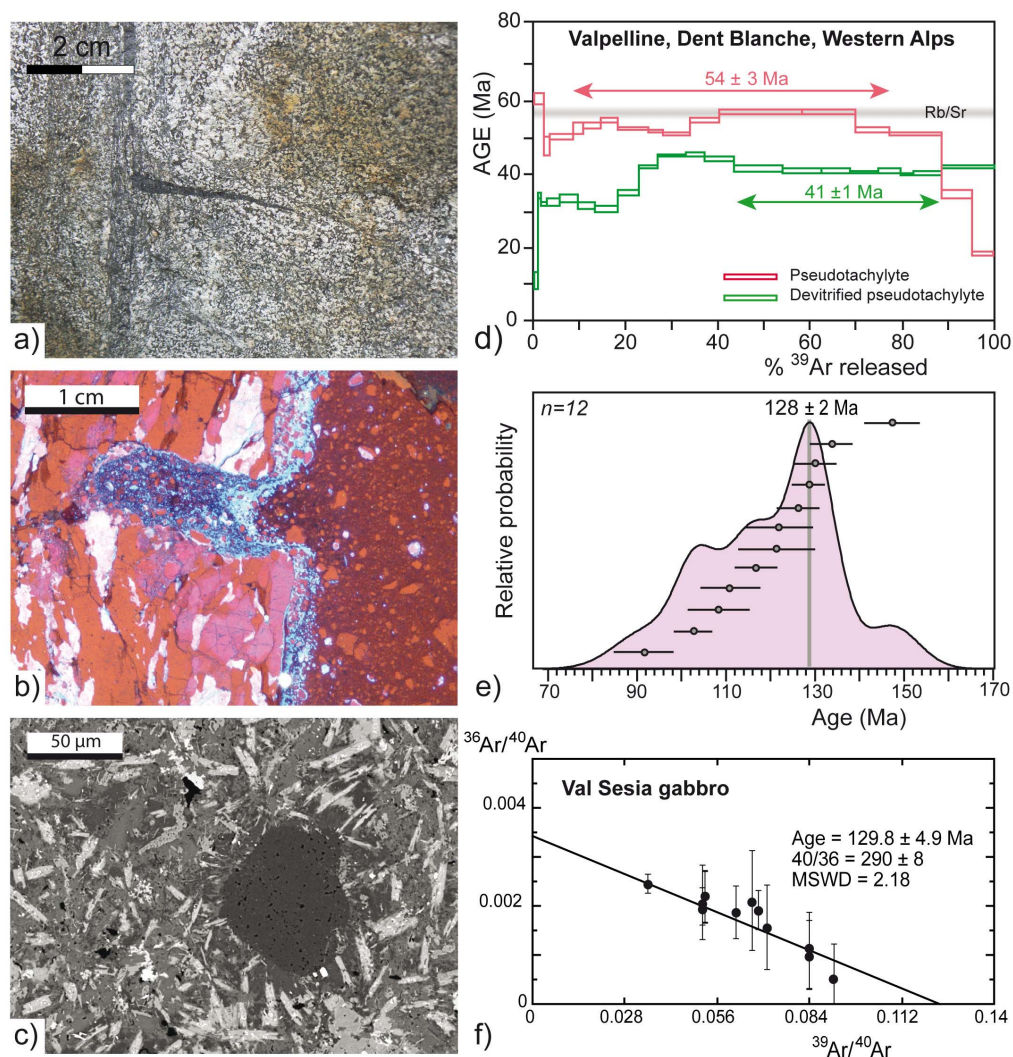


Figure 17. (a) Pseudotachylyte in a gabbro of the Ivrea zone. Note the injection vein perpendicular to the main vein composed of cataclasites on the left and glassy, black pseudotachylyte on the right; (b) Cathodoluminescence image of the contact between a pseudotachylyte vein and a gneiss host-rock cut by an injection vein (Dora Maira). The melt glass (in blue) is concentrated at the very contact with the undeformed host-rock and within the injection vein; (c) BSE image of a pseudotachylyte in a paragneiss of the Ivrea zone showing disoriented mica microlites around a corroded quartz; (d) $^{40}\text{Ar}/^{39}\text{Ar}$ age spectra of two pseudotachylyte samples (injection veins) from the Valpelline unit [Dent Blanche, Menant *et al.*, 2018] showing low and high devitrification effects respectively. Note that the age spectrum of the pseudotachylyte (in red) overlaps the Rb–Sr age of phengites in a nearby shear zone; (e) distribution of *in situ* $^{40}\text{Ar}/^{39}\text{Ar}$ dates within the injection vein shown in (a). Relatively large errors are due to the low amount of potassium in the gabbro host-rock [Souquière *et al.*, 2011]; (f) inverse isochron diagram of the same sample showing an agreement between peak and intercept ages and an initial atmospheric $^{40}\text{Ar}/^{36}\text{Ar}$ composition (no excess argon).

Therefore, the $^{40}\text{Ar}/^{39}\text{Ar}$ dating of pseudotachylytes and associated tectonites appears essential to better understand the mechanics of earthquakes and the links with tectonic activity recorded by ductile and brittle faults in the mid to upper crust. The examples of Figure 17 highlight the microstructural complexity of pseudotachylytes and the difficulty to use them as precise $^{40}\text{Ar}/^{39}\text{Ar}$ geochronometer of seismic ruptures. The behavior of this chronometer remains to be better understood and the effects of various parameters will require consideration in future studies, including slip velocity at rupture and amount of generated melt, mechanical and chemical zonation of the veins, lithology and age of the host rock, nature and distribution of clasts and fragments extracted from the host rock, nature and distribution of neo-formed phases, presence of fluids, alteration phases or devitrification effects.

5. Conclusion

This overview of some recent developments in the $^{40}\text{Ar}/^{39}\text{Ar}$ dating of deformation in fault zones shows that the interpretation of geochronological data is not so straightforward and that it must be supported by a good knowledge of the field, and detailed (micro-) structural and petrological data. For ductile deformations at temperature $<500\text{--}550\text{ }^\circ\text{C}$, the different examples reported in Part 3 show that the $^{40}\text{Ar}/^{39}\text{Ar}$ ages recorded by newly formed synkinematic micas (and more rarely amphibole) have to be considered as crystallization ages rather than cooling ages. Frequently, these newly formed minerals are mixed with prekinematic minerals inherited from the original host rock or from an earlier phase of deformation along the fault zone. In this particular case, the *in situ* laser probe $^{40}\text{Ar}/^{39}\text{Ar}$ method is very powerful since it allows the dating of the different K-bearing mineral generations identified on microstructural and chemical grounds. The behavior of the inherited minerals is strongly dependent on the P – T -fluids conditions that prevail during deformation, on the size and chemistry of these minerals, on the presence or not of short diffusion pathways, on the closed/open system behavior of the studied tectonites. In some favorable geological setting, the K–Ar chronometer of inherited minerals can be fully reset while in other cases, only a limited resetting can be observed. For deeper conditions of deformation (e.g.

high-pressure low temperature terranes), the closed-open system behavior of the host rock can be an critical parameter to consider since it can result in excess argon contamination of the newly crystallized minerals due to limited fluid mobility in a closed system [Laurent *et al.*, 2017]. For all these situations, the integration of $^{40}\text{Ar}/^{39}\text{Ar}$ dates with independent geochronometers (Rb–Sr, U–Pb) may be particularly useful for reconstructing P – T – d – t paths in deformed rocks.

For brittle faults, clays from fault gouges are the first choice target for $^{40}\text{Ar}/^{39}\text{Ar}$ investigations. However, due to ^{39}Ar recoil effect during irradiation, to complex mixture in the fault gouge of minerals with different age, polytype and crystallinity, to complex fluid rock interactions, the interpretation of $^{40}\text{Ar}/^{39}\text{Ar}$ data is not always simply a matter of processing a binary mixture between a single generation of 2M_1 phyllosilicate inherited from the host rock and an authigenic 1M clay synkinematic fraction. By contrast with the K–Ar, the $^{40}\text{Ar}/^{39}\text{Ar}$ step-heating method has the potential to reveal the different argon reservoirs that contribute to the argon release and to eliminate samples with a too complex isotopic signature, such as those contaminated by excess argon. The step-heating approach can also bring information on complex mixtures of inherited and authigenic phyllosilicates in fault gouges with a multiphase activity. The coupling of $^{40}\text{Ar}/^{39}\text{Ar}$ studies in fault gouges with multimethod thermochronological studies (fission tracks, U–Th–Sm/He) in the host rocks may shed light on this repeated motion of brittle faults during exhumation processes using thermal and tectonic modeling (QTQt, Pecube). This aspect remains to be more systematically explored in orogens.

Conflicts of interest

Authors have no conflict of interest to declare.

Acknowledgements

Part of this work (pseudotachylytes, Têt fault) has received fundings from different research programs (3F, TelluS) of the Institut National des Sciences de l'Univers, CNRS. Stéphane Scaillet, Michel Faure and an anonymous reviewer are thanked for their comments that improved the quality of a first manuscript.

References

- Abd Elmola, A., Buatier, M., Monié, P., Labaume, P., Trap, P., and Charpentier, D. (2018). $^{40}\text{Ar}/^{39}\text{Ar}$ muscovite dating of thrust activity: a case study from the Axial Zone of the Pyrenees. *Tectonophysics*, 745, 412–429.
- Abd Elmola, A., Monié, P., Labaume, P., Teixell, A., Charpentier, D., and Buatier, M. (2022). Deformation conditions and $^{40}\text{Ar}/^{39}\text{Ar}$ dating of thrusting recorded by clay minerals: An example of the Lakora thrust (west-central Pyrenees). *J. Struct. Geol.*, 165, article no. 104744.
- Agard, P., Monié, P., Jolivet, L., and Goffé, B. (2002). Exhumation of the Schistes Lustrés complex: *in situ* laser probe $^{40}\text{Ar}/^{39}\text{Ar}$ constraints and implications for the Western Alps. *J. Metamorph. Geol.*, 20, 599–618.
- Allaz, J., Engi, M., Berger, A., and Villa, I. M. (2011). The effects of retrograde reactions and of diffusion on ^{40}Ar – ^{39}Ar ages of micas. *J. Petrol.*, 52, 691–716.
- Allen, A. R. and Stubbs, D. (1982). An $^{40}\text{Ar}/^{39}\text{Ar}$ Ar study of a polymetamorphic complex in the Arunta block, Central Australia. *Contrib. Mineral. Petrol.*, 79, 319–332.
- Angiboust, S., Cambeses, A., Hyppolito, T., Glodny, J., Monié, P., Calderon, M., and Juliani, C. (2018). A 100-m.y.-long window onto mass-flow processes in the Patagonian Mesozoic subduction zone (Diego de Almagro Island, Chile). *Geol. Soc. Am. Bull.*, 130, 1439–1456.
- Angiboust, S., Kirsch, J., Oncken, O., Glodny, J., Monié, P., and Rybacki, E. (2015). Probing the transition between seismically coupled and decoupled segments along an ancient subduction interface. *Geochem. Geophys. Geosyst.*, 16(6), 1905–1922.
- Augier, R., Agard, P., Monié, P., Jolivet, L., Robin, C., and Booth-Rea, G. (2005). Exhumation, doming and slab retreat in the Betic Cordillera (SE Spain): *in situ* $^{40}\text{Ar}/^{39}\text{Ar}$ ages and *P–T–d–t* paths for the Nevado-Filabride complex. *J. Metamorph. Geol.*, 23, 357–381.
- Aumar, C., Merle, O., Bosse, V., and Monié, P. (2022). Syn-rift deformation in the Agly Variscan Massif (Eastern Pyrenees). *BSGF-Earth Sci. Bull.*, 193, article no. 6.
- Avé Lallemand, H. G., Schmidt, W. J., and Kraft, J. L. (1985). Major Late-Triassic strike-slip displacement in the Seven Devils terrane, Oregon and Idaho: a result of left-oblique plate convergence. *Tectonophysics*, 119, 299–328.
- Beaudoin, A., Scaillet, S., Mora, N., Jolivet, L., and Augier, R. (2020). *In situ* and step-heating $^{40}\text{Ar}/^{39}\text{Ar}$ dating of white mica in low-temperature shear zones (Tenda Massif, Alpine Corsica, France). *Tectonics*, 39, 1–35.
- Bellanger, M., Augier, R., Bellahsen, N., Jolivet, L., Monié, P., Baudin, T., and Beyssac, O. (2015). Shortening of the European Dauphinois margin (Oisans massif, Western Alps): New insights from RSCM maximum temperature estimates and $^{40}\text{Ar}/^{39}\text{Ar}$ *in situ* dating. *J. Geodyn.*, 8, 37–64.
- Berger, A. Z., Wehrens, P., Lanari, P., Zwingmann, H., and Herwegh, M. (2017). Microstructures, mineral chemistry and geochronology along a retrograde evolution: an example from the Aar massif (Central Alps, Switzerland). *Tectonophysics*, 721, 179–195.
- Bosse, V. and Villa, I. M. (2019). Petrochronology and hydrochronology of tectono-metamorphic events. *Gondwana Res.*, 71, 76–90.
- Boutin, A., de Saint Blanquat, M., Poujol, M., Boulvais, P., De Parseval, P., Rouleau, C., and Robert, J.-F. (2016). Succession of Permian and Mesozoic metamorphic events in the eastern Pyrenees with emphasis on the Trimouns talc–chlorite deposit. *Int. J. Earth Sci.*, 105, 747–770.
- Brichau, S., Respaut, J. P., and Monié, P. (2007). New age constraints on emplacement of the Cévenol granitoids, South French Massif Central. *Int. J. Earth Sci. (Geol Rundsch)*, 97, 725–738.
- Carreras, J., Czeck, D., Druguet, E., and Hudleston, P. (2010). Structure and development of an anastomosing network of ductile shear zones. *J. Struct. Geol.*, 32, 656–666.
- Carreras, J., Estrada, A., and White, S. (1977). The effects of folding on the C-axis fabrics of a quartz mylonite. *Tectonophysics*, 39, 3–24.
- Chew, D. M., Sylvester, P. J., and Tubrett, M. (2011). U–Pb and Th–Pb dating of apatite by LA-ICPMS. *Chem. Geol.*, 280(1–2), 200–216.
- Chopin, C. and Maluski, H. (1980). ^{40}Ar – ^{39}Ar dating of high-pressure metamorphic micas from the Gran Paradiso area (Western Alps): evidence against the blocking temperature concept. *Contrib. Mineral. Petrol.*, 74, 109–122.
- Clauer, N. (2013). The K–Ar and $^{40}\text{Ar}/^{39}\text{Ar}$ methods revisited for dating fine-grained K-bearing clay minerals. *Chem. Geol.*, 354, 163–185.

- Clauer, N., Zwingmann, H., Liewig, N., and Wendling, R. (2012). Comparative $^{40}\text{Ar}/^{39}\text{Ar}$ and K–Ar dating of illite-type clay minerals: A tentative explanation for age identities and differences. *Earth Sci. Rev.*, 115, 76–96.
- Costa, S. and Maluski, H. (1988). Use of the ^{40}Ar – ^{39}Ar stepwise heating method for dating mylonite zones: An example from the St. Barthélémy massif (Northern Pyrenees, France). *Chem. Geol., Isotope Geosci. Section*, 72, 127–144.
- Dallmeyer, R. D. (1975). $^{40}\text{Ar}/^{39}\text{Ar}$ ages of biotite and hornblende from a progressively remetamorphosed basement terrane: their bearing on interpretation of release spectra. *Geochim. Cosmochim. Acta*, 39, 1655–1669.
- Dallmeyer, R. D., Gee, D. C., and Beckholmen, M. (1985). $^{40}\text{Ar}/^{39}\text{Ar}$ mineral age record of early Caledonian tectonothermal activity in the Baltoscandian miogeosyncline, central Scandinavia. *Am. J. Sci.*, 285, 532–568.
- Di Vincenzo, G., Carosi, R., Palmeri, R., and Tiepolo, M. (2007). A comparative U–Th–Pb (zircon-monazite) and ^{40}Ar – ^{39}Ar (muscovite-biotite) study of shear zones in northern Victoria Land (Antarctica): Implications for geochronology and localized reworking of the Ross Orogen. *J. Metamorph. Geol.*, 25, 605–630.
- Di Vincenzo, G., Ghiribelli, B., Giorgetti, G., and Palmeri, R. (2001). Evidence of a close link between petrology and isotope records: constraints from SEM, EMP, TEM and in situ ^{40}Ar – ^{39}Ar analyses on multiple generations of white micas (Lanternman Range, Antarctica). *Earth Planet. Sci. Lett.*, 192, 389–405.
- Di Vincenzo, G., Godard, G., and Molli, G. (2022). Dating low-grade deformation: role of lithology and strain partitioning on Ar isotope records in the Alpi Apuane of Northern Apennines (Italy). *Tectonics*, 41, article no. e2022TC007248.
- Di Vincenzo, G., Grande, A., Prosser, G., Cavazza, W., and DeCelles, P. G. (2016). ^{40}Ar – ^{39}Ar laser dating of ductile shear zones from central Corsica (France): Evidence of Alpine (middle to late Eocene) synburial shearing in Variscan granitoids. *Lithos*, 262, 369–383.
- Di Vincenzo, G., Rocchi, S., Rossetti, F., and Storti, F. (2004). ^{39}Ar – ^{40}Ar dating of pseudotachylytes: the effect of clast-hosted extraneous argon in Cenozoic fault-generated friction melts from the West Antarctic Rift System. *Earth Planet. Sci. Lett.*, 223, 349–364.
- Dodson, M. H. (1973). Closure temperature in cooling geochronological and petrological systems. *Contrib. Mineral. Petrol.*, 40, 259–274.
- Dong, H., Hall, C. M., Peacor, D. R., and Halliday, A. N. (1995). Mechanisms of argon retention in layers revealed by laser ^{40}Ar – ^{39}Ar dating. *Science*, 267, 355–359.
- Druguet, E., Alsop, G., and Carreras, J. (2009). Coeval brittle and ductile structures associated with extreme deformation partitioning in a multilayer sequence. *J. Struct. Geol.*, 3, 498–511.
- Druguet, E., Castro, A., Chichorro, M., Pereira, M. F., and Fernandez, C. (2014). Zircon geochronology of intrusive rocks from Cap de Creus, Eastern Pyrenees. *Geol. Mag.*, 151, 1–20.
- Druguet, E., Passchier, C., Carreras, J., Victor, P., and den Brok, B. (1997). Analysis of a complex high-strain zone at Cap de Creus, Spain. *Tectonophysics*, 280, 31–45.
- Duvall, A., Clark, M., van der Pluijm, B., and Li, C. (2011). Direct dating of Eocene reverse faulting in northeastern Tibet using Ar-dating of fault clays and low temperature thermochronometry. *Earth Planet. Sci. Lett.*, 304, 520–526.
- Faure, G. and Mensing, T. M. (2004). *Isotopes: Principles and Applications*. Wiley, Hoboken, 3rd edition. 897 p. ISBN: 978-0-471-38437-3.
- Ferkous, K. and Monié, P. (2002). Neoproterozoic shearing and auriferous hydrothermalism along the lithospheric N–S In Ouzzal shear zone (Western Hoggar, Algeria, North Africa). *J. Afr. Earth. Sci.*, 35, 399–415.
- Fernandez, L., Bosch, D., Bruguier, O., Hammor, D., Caby, R., Arnaud, N., Monié, P., Abdallah, N., Verdoux, P., Ouabadi, A., and Laouar, R. (2020). Vestiges of a fore-arc oceanic crust in the Western Mediterranean: Geochemical constraints from North-East Algeria. *Lithos*, 370–371, article no. 105649.
- Fitch, F. J., Miller, J. A., and Mitchell, J. G. (1969). A new approach to radio-isotope dating in orogenic belts. In Kent, P. E., Satterthwaite, G. E., and Spencer, A. M., editors, *Time and Place in Orogeny*, volume 3 of *Geological Society, London, Special Publications*, pages 157–195. Geological Society of London.
- Fitz-Diaz, E., Hall, C. M., and van der Pluijm, B.

- (2016). XRD-based $^{40}\text{Ar}/^{39}\text{Ar}$ age correction for fine-grained illite, with application to folded carbonates in the Monterrey Salient (northern Mexico). *Geochim. Cosmochim. Acta*, 181, 201–216.
- Fleck, R., Calvert, A., Coble, M. A., Wooden, J., Hodges, K., Hayden, L., van Soest, M., Bray, E., and John, D. (2019). Characterization of the rhyolite of Bodie Hills and $^{40}\text{Ar}/^{39}\text{Ar}$ intercalibration with Ar mineral standards. *Chem. Geol.*, 525, 282–302.
- Foland, K. A., Hubacher, F. A., and Arehart, G. B. (1992). $^{40}\text{Ar}/^{39}\text{Ar}$ dating of very fine-grained samples: An encapsulated-vial procedure to overcome the problem of ^{39}Ar recoil loss. *Chem. Geol.*, 102(1–4), 269–276.
- Freed, R. L. and Peacor, D. R. (1989). Variability in temperature of the smectite/illite reaction in Gulf Coast sediments. *Clay Miner.*, 24, 171–180.
- Gemignani, L., Kuiper, K. F., Wijbrans, J. R., Sun, X., and Santato, A. (2018). Improving the precision of single grain mica $^{40}\text{Ar}/^{39}\text{Ar}$ dating on smaller and younger muscovite grains: Application to provenance studies. *Chem. Geol.*, 511, 100–111.
- Ghignone, S., Sudo, M., Balestro, G., Borghi, A., Gattiglio, M., Ferrero, S., and Schijndel, V. (2021). Timing of exhumation of meta-ophiolite units in the Western Alps: New tectonic implications from $^{40}\text{Ar}/^{39}\text{Ar}$ white mica ages from Piedmont Zone (Susa Valley). *Lithos*, 404–405, article no. 106443.
- Haines, S. H. and van der Pluijm, B. A. (2008). Clay quantification and Ar–Ar dating of synthetic and natural gouge: application to the Miocene Sierra Mazatán detachment fault, Sonora, Mexico. *J. Struct. Geol.*, 30(4), 525–538.
- Haines, S. H. and van der Pluijm, B. A. (2010). Dating the detachment fault system of the Ruby Mountains, Nevada: Significance for the kinematics of low-angle normal faults. *Tectonics*, 29, article no. TC4028.
- Haines, S. H. and van der Pluijm, B. A. (2012). Patterns of mineral transformations in clay gouge, with examples from low-angle normal fault rocks in the western USA. *J. Struct. Geol.*, 43, 2–32.
- Hall, C. M. (2015). Direct measurement of recoil effects on $^{40}\text{Ar}/^{39}\text{Ar}$ standards. In Jourdan, F., Mark, D. F., and Verati, C., editors, *Advances in $^{40}\text{Ar}/^{39}\text{Ar}$ Dating: From Archaeology to Planetary Sciences*, volume 378 of *Geological Society, London, Special Publications*, pages 53–62. Geological Society of London.
- Hall, C. M., Higuera, P., Kesler, S. E., Lunar, R., Dong, H., and Halliday, A. N. (1997). Dating of alteration episodes related to mercury mineralization in the Almadén district, Spain. *Earth Planet. Sci. Lett.*, 148, 287–298.
- Hall, C. M., Kesler, S., Simon, G., and Fortuna, J. (2000). Overlapping Cretaceous and Eocene alteration, Twin Creeks Carlin-type deposit, Nevada. *Econ. Geol.*, 95, 1739–1752.
- Hames, W. E. and Bowring, S. A. (1994). An empirical evaluation of the argon diffusion geometry in muscovite. *Earth Planet. Sci. Lett.*, 124, 161–167.
- Hames, W. E. and Hodges, K. V. (1993). Laser $^{40}\text{Ar}/^{39}\text{Ar}$ evaluation of slow cooling and episodic loss of ^{40}Ar from a sample of polymetamorphic muscovite. *Science*, 261, 1721–1723.
- Harrison, T. M., Catlos, E. J., and Montel, J. M. (2002). U–Th–Pb dating of phosphate minerals. *Rev. Mineral.*, 48, 523–558.
- Harrison, T. M., Célérier, J., Aikman, A. B., Hermann, J., and Heizler, M. T. (2009). Diffusion of ^{40}Ar in muscovite. *Geochim. Cosmochim. Acta*, 73, 1039–1051.
- Hodges, K. V., Hames, W. E., and Bowring, S. A. (1994). $^{40}\text{Ar}/^{39}\text{Ar}$ age gradients in micas from a high-temperature low-pressure metamorphic terrain: Evidence for very slow cooling and implications for the interpretation of age spectra. *Geology*, 22, 55–58.
- Hubbard, M. S. and Harrison, T. M. (1989). $^{40}\text{Ar}/^{39}\text{Ar}$ age constraints on deformation and metamorphism in the MCT zone and Tibetan slab, eastern Nepal Himalaya. *Tectonics*, 8, 865–880.
- Huet, B., Labrousse, L., Monié, P., Malvoisin, B., and Jolivet, L. (2015). Coupled phengite ^{40}Ar – ^{39}Ar geochronology and thermobarometry: *P–T–t* evolution of Andros Island (Cyclades, Greece). *Geol. Mag.*, 152, 711–727.
- Jourdan, F., Mark, D. F., and Verati, C. (2014). *Advances in $^{40}\text{Ar}/^{39}\text{Ar}$ Dating: From Archaeology to Planetary Sciences*, volume 378 of *Geological Society, London, Special Publications*. Geological Society of London.
- Kellett, D. A., Warren, C., Larson, K., Zwingmann, H., van Staal, C. R., and Rogers, N. (2016). Influence of deformation and fluids on Ar retention in white mica: Dating the Dover Fault, Newfoundland Appalachians. *Lithos*, 254–255, 1–17.
- Kelley, S. P., Bartlett, J. M., and Harris, N. B. W. (1997).

- Pre-metamorphic Ar–Ar ages from biotite inclusions in garnet. *Geochim. Cosmochim. Acta*, 61, 3873–3878.
- Keppie, J. D. and Dallmeyer, R. D. (1987). Dating transcurrent terrane accretion: An example from the Meguma and Avalon Composite Terranes in the northern Appalachians. *Tectonics*, 6, 831–847.
- Kligfield, R., Hunziker, J., and Schame, S. (1986). Dating of deformation phases using K–Ar and $^{40}\text{Ar}/^{39}\text{Ar}$ techniques: results from the northern Apennines. *J. Struct. Geol.*, 8, 781–798.
- Kramar, N., Cosca, M., and Hunziker, J. (2001). Heterogeneous $^{40}\text{Ar}^*$ distributions in naturally deformed muscovite: in situ UV-laser ablation evidence for microstructurally controlled intragrain diffusion. *Earth Planet. Sci. Lett.*, 192, 377–388.
- Lanari, P., Rolland, Y., Schwartz, S., Vidal, O., Guillot, S., Tricart, P., and Dumont, T. (2014). P – T – t estimation of deformation in low-grade quartz-feldspar-bearing rocks using thermodynamic modelling and $^{40}\text{Ar}/^{39}\text{Ar}$ dating techniques: example of the Plan-de-Phasy shear zone unit (Briançonnais Zone, Western Alps). *Terra Nova*, 26(2), 130–138.
- Laurent, V., Huet, B., Labrousse, L., Jolivet, L., Monié, P., and Augier, R. (2017). Extraneous argon in high-pressure metamorphic rocks: Distribution, origin and transport in the Cycladic Blueschist Unit (Greece). *Lithos*, 272–273, 315–335.
- Li, W., Cao, S., Zhan, L., Cheng, X., Li, W., and Lyu, M. (2022). Crush-origin pseudotachylyte in granitic mylonites of continental exhumed Ailaoshan-Red River shear zone, southeastern Asia. *J. Struct. Geol.*, 159, article no. 104606.
- Lin, L. H., Onstott, T. C., and Dong, H. (2000). Backscattered ^{39}Ar loss in fine-grained minerals: Implications for $^{40}\text{Ar}/^{39}\text{Ar}$ geochronology of clay. *Geochim. Cosmochim. Acta*, 64(23), 3965–3974.
- Lo, C. H., Lee, J. K. W., and Onstott, T. C. (2000). Argon release mechanisms of biotite *in vacuo* and the role of short-circuit diffusion and recoil. *Chem. Geol.*, 165, 135–166.
- Ludwig, K. R. (2012). *User's Manual for Isoplot Version 3.75–4.15: A Geochronological Toolkit for Microsoft Excel*. Berkeley Geochronological Center Special Publication, 5, Berkeley, California. 72 p.
- Malusà, M. G. and Fitzgerald, P. G. (2019). Application of thermochronology to geologic problems: bedrock and detrital approaches. In Malusà, M. G. and Fitzgerald, P. G., editors, *Fission-Track Thermochronology and its Application to Geology*. Springer, Berlin.
- Maluski, H. and Monié, P. (1988). ^{40}Ar – ^{39}Ar laser probe multi-dating inside single biotites of a Variscan orthogneiss (Pinet, Massif Central, France). *Chem. Geol.*, 73, 245–263.
- Maluski, H. and Schaeffer, O. A. (1981). Utilisation d'une sonde laser pour l'analyse des minéraux par la méthode ^{39}Ar – ^{40}Ar . *Bull. Soc. Géol. Fr.*, 7, 401–407.
- Maurel, O., Monié, P., Respaut, J. P., Leyreloup, A. E., and Maluski, H. (2003). Pre-metamorphic $^{40}\text{Ar}/^{39}\text{Ar}$ and U–Pb ages in HP metagranitoids from the Hercynian belt (France). *Chem. Geol.*, 193, 195–214.
- McCaig, A. M. and Miller, J. A. (1986). ^{40}Ar – ^{39}Ar age of mylonites along the Merens Fault, central Pyrenees. *Tectonophysics*, 129, 149–172.
- McDonald, C. S., Warren, C. J., Mark, D. F., Halton, A. M., Kelley, S. P., and Sherlock, S. C. (2016). Argon redistribution during a metamorphic cycle: Consequences for determining cooling rates. *Chem. Geol.*, 443, 182–197.
- McDougall, I. and Harrison, T. M. (1999). *Geochronology and Thermochronology by the $^{40}\text{Ar}/^{39}\text{Ar}$ Method*. Oxford University Press, New York, 2nd edition. 269 p.
- Megrué, G. H. (1973). Spatial distribution of $^{40}\text{Ar}/^{39}\text{Ar}$ ages in lunar breccia 14301. *J. Geophys. Res.*, 78, 3216–3221.
- Menant, A., Angiboust, S., Monié, P., Oncken, O., and Guigner, J. M. (2018). Brittle deformation during Alpine basal accretion and the origin of seismicity nests above the subduction interface. *Earth Planet. Sci. Lett.*, 487, 84–93.
- Merrihue, C. and Turner, G. (1966). Potassium-argon dating by activation with fast neutrons. *J. Geophys. Res.*, 71, 2852–2857.
- Milesi, G. (2020). Analyse thermochronologique, géochimique et structurale du système hydrothermal de la faille de la Têt (Pyrénées, France): un nouvel outil d'exploration géothermique. Doctoral dissertation, University Montpellier. HAL Id: tel-0334031.
- Milesi, G., Charpentier, D., Monié, P., Leclère, H., Münch, P., Bouaoudi, A., Buatier, M., Trap, P., Soliva, R., and Iemmolo, A. (2022). Dating fault activity in the eastern part of the Pyrenees: a com-

- bined approach low-temperature thermochronology and $^{40}\text{Ar}/^{39}\text{Ar}$. In *XVII ICC Istanbul 2022*, volume 158.
- Mitterperger, S., Zanchetta, S., Caldiroli, F., Zanchi, A., Bistacchi, A., Hanchar, J., and Villa, I. (2022). The timescale of solid-state deformation in the Northern Adamello igneous intrusive suite. *J. Geol. Soc. Lond.*, 179(4), article no. jgs2021-101.
- Monié, P., Caby, R., and Maluski, H. (1984). ^{39}Ar - ^{40}Ar investigations within the Grande Kabylie massif (northern Algeria): evidences for its Alpine structuration. *Eclogae Geol. Helv.*, 77, 115–141.
- Monié, P., Oliot, E., Faucher, A., and Allard, M. (2018). Age Eocène $^{40}\text{Ar}/^{39}\text{Ar}$ des zones de cisaillement de basse température dans la péninsule du Cap de Creus, NW Espagne. In *Conséquences géodynamiques. Talk. Congrès Réunion des Sciences de la Terre RST 26th edition, Lille*.
- Monié, P., Soliva, J., Brunel, M., and Maluski, H. (1994). Les cisaillements mylonitiques du granite de Millas (Pyrénées, France); âge Crétacé $^{40}\text{Ar}/^{39}\text{Ar}$ et interprétation tectonique. *Bull. Soc. Géol. Fr.*, 16, 559–571.
- Montmartin, C. (2021). Métamorphisme tardi-orogénique dans le domaine externe d'une chaîne de montagnes. Nouvelles contraintes par thermométrie RSCM et datation $^{40}\text{Ar}/^{39}\text{Ar}$ dans le sud de chaîne varisque (Cévennes et Montagne Noire). Thèse doctorat Univ. Orléans, HAL Id: tel-03360303.
- Mulch, A., Cosca, M., and Handy, M. (2002). In-situ UV-laser $^{40}\text{Ar}/^{39}\text{Ar}$ geochronology of a micaceous mylonite: An example of defect-enhanced argon loss. *Contrib. Mineral. Petrol.*, 142, 738–752.
- Mulch, A. and Cosca, M. A. (2004). Recrystallization or cooling ages: UV-laser $^{40}\text{Ar}/^{39}\text{Ar}$ geochronology of muscovite in mylonitic rocks. *J. Geol. Soc. Lond.*, 161, 573–582.
- Mulch, A., Cosca, M. A., Andrese, A., and Fiebig, J. (2005). Time scales of deformation and exhumation in extensional detachment systems determined by high-spatial resolution in situ UV-laser $^{40}\text{Ar}/^{39}\text{Ar}$ dating. *Earth Planet. Sci. Lett.*, 233, 375–390.
- Müller, W., Kelley, S. P., and Villa, I. M. (2002). Dating fault-generated pseudotachylytes: comparison of $^{40}\text{Ar}/^{39}\text{Ar}$ stepwise-heating, laser-ablation and Rb-Sr microsampling analyses. *Contrib. Mineral. Petrol.*, 144, 57–77.
- Münch, P., Caillaud, J., Monié, P., Grauby, O., Corsini, M., Ricci, J., Romagny, A., Philippon, M., Lanson, B., Azdimousa, A., Ben Moussa, A., and Arnaud, N. (2021). Direct dating of brittle extensional deformation contemporaneous of Neogene exhumation of the internal zones of the Rif Chain. *Tectonophysics*, 807, article no. 228800.
- Naumenko-Dèzes, M. O., Villa, I. M., Rolland, Y., Gallet, S., and Lanari, P. (2021). Subgrain $^{40}\text{Ar}/^{39}\text{Ar}$ dating of museum-quality micas reveals intragrain heterogeneity. *Chem. Geol.*, 573, article no. 120215.
- Nteme, J., Scaillet, S., Brault, P., and Tassan-Got, L. (2022). Atomistic simulations of ^{40}Ar diffusion in muscovite. *Geochim. Cosmochim. Acta*, 331, 123–142.
- Okay, A. I. and Monié, P. (1997). Early Mesozoic subduction in the Eastern Mediterranean: Evidence from Triassic eclogites in northwest Turkey. *Geology*, 25, 595–598.
- Onstott, T. C., Miller, M. L., Ewing, R. C., Arnold, G. W., and Walsh, D. S. (1995). Recoil refinements: implications for the ^{40}Ar - ^{39}Ar dating technique. *Geochim. Cosmochim. Acta*, 59(9), 1821–1834.
- Oriolo, S., Wemmer, K., Oyhantçabal, P., Fossen, H., Schulz, B., and Siegesmund, S. (2018). Geochronology of shear zones—A review. *Earth Sci. Rev.*, 185, 665–683.
- Parrish, R. R. (1990). U-Pb dating of monazite and its application to geological problems. *Can. J. Earth. Sci.*, 27, 1431–1450.
- Parry, W. T., Bunds, M. P., Bruhn, R. L., Hall, C. M., and Murphy, J. M. (2001). Mineralogy, $^{40}\text{Ar}/^{39}\text{Ar}$ dating and apatite fission track dating of rocks along the Castle Mountain fault, Alaska. *Tectonophysics*, 337, 149–172.
- Pevear, D. R. (1999). Illite and hydrocarbon exploration. *Proc. Natl Acad. Sci.*, 96, 3440–3446.
- Phillips, D. (1991). Argon isotope and halogen chemistry of phlogopite from South African kimberlites: a combined step-heating, laser probe, electron microprobe and TEM study. *Chem. Geol.*, 87, 71–98.
- Phillips, D. and Onstott, T. C. (1988). Argon isotopic zoning in mantle phlogopite. *Geology*, 16(6), 542–546.
- Porkoláb, K., Matenco, L., Hupkes, J., Willingshofer, E., Wijbrans, J., van Schroyen Lantman, H., and van Hinsbergen, D. J. J. (2022). Tectonic evolution of the Nevado-Filábride Complex (Sierra de

- Los Filábres, southeastern Spain): Insights from new structural and geochronological data. *Tectonics*, 41, article no. e2021TC006922.
- Reuter, A. and Dallmeyer, R. D. (1987). $^{40}\text{Ar}/^{39}\text{Ar}$ age spectra of whole rock and constituent grain size fractions from anchizonal slates. *Chem. Geol.*, 66, 73–88.
- Ring, U., Uysal, I. T., Glodny, J., Cox, S. C., Little, T., Thomson, S. N., and Bozkaya, Ö. (2017). Fault-gouge dating in the Southern Alps, New Zealand. *Tectonophysics*, 717, 321–338.
- Roberts, N. M. W. and Holdsworth, R. E. (2022). Timescales of faulting through calcite geochronology: A review. *J. Struct. Geol.*, 158, article no. 104578.
- Rolland, Y., Rossi, M., Cox, S. F., Corsini, M., Mancktelow, N., Pennacchioni, G., Fornari, M., and Boullier, A. M. (2008). $^{40}\text{Ar}/^{39}\text{Ar}$ dating of synkinematic white mica: insights from fluid-rock reaction in low-grade shear zones (Mont Blanc Massif) and constraints on timing of deformation in the NW external Alps. In Wibberley, C. A. J., Kurz, W., Imber, J., Holdsworth, R. E., and Collettini, C., editors, *The Internal Nature of Fault Zones: Implications for Mechanical and Fluid-Flow Properties*, volume 299 of *Geological Society, London, Special Publications*, pages 293–315. Geological Society of London.
- Roques, C., Weber, U. W., Brixel, B., Krietsch, H., Dutler, N., Brennwald, M. S., and Kipfer, R. (2020). In situ observation of helium and argon release during fluid-pressure-triggered rock deformation. *Sci. Rep.*, 10, article no. 6949.
- Rösel, D. and Zack, Th. (2021). LA-ICP-MS/MS single-spot Rb-Sr dating. *Geostand. Geoanal. Res.*, 46, 143–168.
- Rossetti, F., Monié, P., Nasrabad, M., Theye, T., Lucci, F., and Saadat, M. (2017). Early Carboniferous subduction-zone metamorphism preserved within the Palaeo-Tethyan Rasht ophiolites (western Alborz, Iran). *J. Geol. Soc. Lond.*, 174, 741–758.
- Sanchez, G., Rolland, Y., Schneider, J., Corsini, M., Oliot, E., Goncalves, P., Verati, C., Lardeaux, J. M., and Marquer, D. (2011). Dating low-temperature deformation on white micas, insight from the Argentera-Mercantour Massif (SW Alps). *Lithos*, 125, 521–536.
- Scaillet, S., Féraud, G., Lagabrielle, Y., Ballèvre, M., and Ruffet, G. (1990). $^{40}\text{Ar}/^{39}\text{Ar}$ laser-probe dating by step-heating and spot-fusion of phengites from the Dora Maira nappe of the western Alps, Italy. *Geology*, 18, 741–744.
- Schaen, A. J. et al. (2021). Interpreting and reporting $^{40}\text{Ar}/^{39}\text{Ar}$ geochronological data. *Geol. Soc. Am. Bull.*, 133, 461–487.
- Scharf, A., Handy, M., Schmid, S., Favaro, S., Sudo, M., Schuster, R., and Hammerschmidt, K. (2016). Grain-size effects on the closure temperature of white mica in a crustal-scale extensional shear zone - Implications of in-situ $^{40}\text{Ar}/^{39}\text{Ar}$ laser-ablation of white mica for dating shearing and cooling (Tauern Window, Eastern Alps). *Tectonophysics*, 674, 210–226.
- Schneider, J., Bosch, D., and Monié, P. (2008). Individualization of textural and reactional microdomains in eclogites from the Bergen Arcs (Norway): Consequences for Rb/Sr and Ar/Ar radiochronometer behaviour during polymetamorphism. *Geochim. Geophys. Geosyst.*, 9, article no. Q12001.
- Schneider, S., Hammerschmidt, K., and Rosenberg, C. (2012). Dating the longevity of ductile shear zones: Insight from $^{40}\text{Ar}/^{39}\text{Ar}$ *in situ* analyses. *Earth Planet. Sci. Lett.*, 369–370, 43–58.
- Sherlock, S. and Hetzel, R. (2001). A laser-probe $^{40}\text{Ar}/^{39}\text{Ar}$ study of pseudotachylite from the Tambauch Fault Zone, Kenya: direct isotopic dating of brittle faults. *J. Struct. Geol.*, 23, 33–44.
- Simon-Labric, T., Rolland, Y., Dumont, T., Heymes, T., Authemayou, C., Corsini, M., and Fornari, M. (2009). $^{40}\text{Ar}/^{39}\text{Ar}$ dating of Penninic Front tectonic displacement (W Alps) during the Lower Oligocene (31–34 Ma). *Terra Nova*, 21(2), 127–136.
- Skipton, D. R., Warren, C. J., and Hanke, F. (2018). Numerical models of P - T , time and grain-size controls on Ar diffusion in biotite: An aide to interpreting $^{40}\text{Ar}/^{39}\text{Ar}$ ages. *Chem. Geol.*, 496, 14–24.
- Sletten, V. W. and Onstott, A. T. (1998). The effect of the instability of muscovite during *in vacuo* heating on $^{40}\text{Ar}/^{39}\text{Ar}$ step-heating spectra. *Geochim. Cosmochim. Acta*, 62(1), 123–141.
- Solum, J., van der Pluijm, B., and Peacor, D. (2005). Neocrystallization, fabrics and age of clay minerals from an exposure of the Moab Fault, Utah. *J. Struct. Geol.*, 27, 1563–1576.
- Souquière, E., Monié, P., Fabbri, O., and Chauvet, A. (2011). Polyphase seismic faulting in the Ivrea zone revealed by $^{40}\text{Ar}/^{39}\text{Ar}$ dating of pseudotachylites. *Terra Nova*, 23, 162–170.

- Tagami, T. (2012). Thermochronological investigation of fault zones. *Tectonophysics*, 538–540, 67–85.
- Tan, Z., Agard, P., Monié, P., Gao, J., John, T., Bayet, L., Jiang, T., Wang, X. S., Hong, T., Wan, B., and Caron, B. (2019). Architecture and *P-T*-deformation-time evolution of the Chinese SW-Tianshan HP/UHP complex: Implications for subduction dynamics. *Earth Sci. Rev.*, 197, article no. 102894.
- Teixell, A., Labaume, P., Ayarz, P., Espurt, N., de Saint Blanquat, M., and Lagabrielle, Y. (2018). Crustal structure and evolution of the Pyrenean-Cantabrian belt: A review and new interpretations from recent concepts and data. *Tectonophysics*, 724–725, 146–170.
- Ternois, S., Odlum, M., Ford, M., Pik, R., Stockli, D., Tibari, B., Vacherat, A., and Bernard, V. (2019). Thermochronological evidence of early orogenesis, Eastern Pyrenees, France. *Tectonics*, 38, 1308–1336.
- Torgersen, E., Gabrielsen, R., Ganerød, M., Van der Lelij, R., Schönerberger, J., Nystuen, J., and Brask, S. (2022). Repeated brittle reactivations of a pre-existing plastic shear zone: Combined K–Ar and ^{40}Ar – ^{39}Ar geochronology of the long-lived (>700 Ma) Himdalen–Ørje Deformation Zone, SE Norway. *Geol. Mag.*, 159, 2110–2131.
- Turrillot, P., Augier, R., Monié, P., and Faure, M. (2011). Late orogenic exhumation of the Variscan high-grade units (South Armorican Domain, western France), combined structural and $^{40}\text{Ar}/^{39}\text{Ar}$ constraints. *Tectonics*, 30, article no. TC 5007.
- Uunk, B., Brouwer, F., ter Voorde, M., and Wijbrans, J. (2018). Understanding phengite argon closure using single grain fusion age distributions in the Cycladic Blueschist Unit on Syros, Greece. *Earth Planet. Sci. Lett.*, 484, 192–203.
- van der Pluijm, B., Hall, C., Vrolijk, P., Pevear, D., and Covey, M. (2001). The dating of shallow faults in the Earth's crust. *Nature*, 412, 172–174.
- van Lichtervelde, M., Grand'Homme, A., de Saint Blanquat, M., Olivier, P., Gerdes, A., et al. (2017). U–Pb geochronology on zircon and columbite-group minerals of the Cap de Creus pegmatites, NE Spain. *Mineral. Petrol.*, 111, 1–21.
- Vanardois, J., Trap, P., Roger, F., Goncalves, P., Marquer, D., Paquette, J. L., Siron, G., and Baudin, T. (2022). Flow of the partially molten crust in the Variscan foreland revealed by U–Th–Pb dating of metamorphism, magmatism and deformation (Agly Massif, Eastern Pyrenees). *Int. J. Earth Sci.*, 111, 2101–2128.
- Vermeesch, P. (2018). IsoplotR: a free and open toolbox for geochronology. *Geosci. Front.*, 9, 1479–1493.
- Villa, I. M. (2016). Diffusion in mineral geochronometers: Present and absent. *Chem. Geol.*, 420, 1–10.
- Villa, I. M. (2021). The *in vacuo* release of Ar from minerals: 1. Hydrous minerals. *Chem. Geol.*, 564, article no. 120076.
- Villa, I. M. (2022). Dating deformation: the role of atomic-scale processes. *J. Geol. Soc. Lond.*, 179, article no. jgs2021-098.
- Villa, I. M., Bucher, S., Bousquet, R., Kleinhanns, I. C., and Schmid, S. M. (2014). Dating polygenetic metamorphic assemblages along a transect across the Western Alps. *J. Petrol.*, 55, 803–830.
- Vissers, R., Ganerød, M., Pennock, G., and van Hinsbergen, D. (2020). Eocene seismogenic reactivation of a Jurassic ductile shear zone at Cap de Creus, Pyrenees, NE Spain. *J. Struct. Geol.*, 134, article no. 103994.
- Vissers, R., van Hinsbergen, D., Wilkinson, C., and Ganerød, M. (2016). Middle Jurassic shear zones at Cap de Creus (eastern Pyrenees, Spain): a record of pre-drift extension of the Piemonte–Ligurian Ocean? *J. Geol. Soc. Lond.*, 174, 289–300.
- Warren, C. J., Hanke, F., and Kelley, S. P. (2012). When can muscovite $^{40}\text{Ar}/^{39}\text{Ar}$ dating constrain the timing of metamorphic exhumation? *Chem. Geol.*, 291, 79–86.
- Wijbrans, J. R. and McDougall, I. (1986). $^{40}\text{Ar}/^{39}\text{Ar}$ dating of white micas from an Alpine high-pressure metamorphic belt on Naxos (Greece): the resetting of the argon isotopic system. *Contrib. Mineral. Petrol.*, 93, 187–194.
- York, D., Hall, C. M., Yanase, Y., Hanes, J. A., and Kenon, J. (1981). ^{40}Ar – ^{39}Ar dating of terrestrial minerals with a continuous laser. *Geophys. Res. Lett.*, 8, 1136–1138.
- Zwingmann, H., Mancktelow, N., Antognini, M., and Lucchini, R. (2010a). Dating of shallow faults: new constraints from the AlpTransit tunnel site (Switzerland). *Geology*, 38, 487–490.
- Zwingmann, H., Yamada, K., and Tagami, T. (2010b). Timing of brittle deformation within the Nojima fault zone, Japan. *Chem. Geol.*, 275, 176–185.